Analysis of mast cells in the neonatal ovary of MRL/MpJ mice –unique immune cells participating in early follicular development–

MRL/MpJ マウスの新生子期卵巣に出現する肥満細胞の解析

–初期卵胞形成に参加する特異な免疫細胞–

Teppei Nakamura

Laboratory of Anatomy

Department of Biomedical Sciences

Graduate School of Veterinary Medicine

Hokkaido University

Abbreviations

Bmp15: *Bone morphogenetic protein 15*

Ccl: *Chemokine (C-C motif) ligand*

cDNA: complementary deoxyribonucleic acid

Chr: chromosome

cM: centimorgan

Cma1, Cma1: Chymase 1

Cpa3, Cpa3: Carboxypeptidase A3

CTMC: connective tissue mast cell

Cx3cl: *Chemokine (C-X3-C motif) ligand*

DDX4: DEAD (Asp-Glu-Ala-Asp) box polypeptide 4

E: embryonic day

Gdf9: *Growth differentiation factor 9*

H&E: hematoxylin and eosin

Il15: *Interleukin 15*

LRS: likelihood ratio statistics

MC: mast cell

Mcpt: Mast cell protease

MMC: mucosal mast cell

Mmp2: *Matrix metallopeptidase 2*

MPD: Mouse Phenome Database

Mt: *Metallothionein*

OMC: ovarian mast cell

P: postnatal day

PCR: polymerase chain reaction

qPCR: quantitative real-time PCR

QTL: quantitative trait locus

RNA: ribonucleic acid

RT-PCR: reverse transcription PCR

SE: surface epithelium

SEM: standard error of the mean

SNP: single nucleotide polymorphism

TB: toluidine blue

Tex101:*Testis-expressed gene 101*

TNF-α: Tumor necrosis factor-α

Tpsab1, Tpsab1: Tryptase alpha/beta 1

Tpsb2, Tpsb2: Tryptase beta 2

Zp: *Zona pellucida glycoprotein*

Indexes

Preface

The Murphy Roths Large (MRL/MpJ) mice originate from C57BL/6J (0.3%), C3H/HeDi (12.1%), AKR/J (12.6%), and LG/J (75.0%) strains. MRL/MpJ mice and their mutant strain, MRL/MpJ-*lpr/lpr* mice, are models for autoimmune diseases that resemble human systemic lupus erythematosus and rheumatoid arthritis (Theofilopoulos and Dixon 1985; Nose et al. 2000). In addition to autoimmune phenotypes, MRL/MpJ mice show some unique phenotypes related to wound healing, such as accelerated ear punch closure and cardiomyocyte regeneration (Clark et al. 1998; Leferovich et al. 2001; Yu et al. 2005). This strain also shows unique characteristics in the reproductive organs; *i.e.*, metaphase-specific apoptosis of meiotic spermatocytes (Kon et al. 1999; Kon and Endoh 2000), heat shock resistance of spermatocytes found in experimental cryptorchidism (Kon and Endoh 2001), existence of testicular oocytes in newborn males (Otsuka et al. 2008ab), and development of ovarian cysts originating from the rete ovarii (Kon et al. 2007). Interestingly, in this study, the author found that MRL/MpJ mice possess numerous mast cells (MCs) in their neonatal ovary.

MCs reside in most tissues and act as sentinel cells in both innate and adaptive immunity (Galli et al. 2005ab). In several species including human, the reproductive organs of adult females have different immune cells, such as macrophages, neutrophils, eosinophils, and MCs (Gaytán et al. 1991; Brännström et al. 1993; Norman and Brännström 1994; Cavender and Murdoch 1988). In addition, the abnormality of immune system such as autoimmune diseases could be a risk factor of development of female infertility (Silva et al. 2014). It has also been reported that MCs accumulate in

mammary glands, placentas, uteri, and ovaries (Krishna et al. 1989; Rudolph et al. 2004; Ramirez et al. 2012; Woidacki et al. 2013). The appearance of these immune cells is altered by the sex hormones during the estrus cycle or pregnancy, indicating that MCs play some important roles in reproductive functions. Furthermore, the appearance of MCs before sexual maturation has been shown in the ovaries of neonatal ICR mice (Skalko et al. 1968). However, the morphological characteristics of the ovarian MCs in the neonetal ovary and the functional relationship between MCs and the perinatal ovary are still unclear.

Therefore, the author considered that neonatal MRL/MpJ mice, possessing numerous ovarian MC, would be useful to examine the relationship between immune system and ovary, especially in early follicular development. This thesis contains two chapters; the first chapter provides the morphology of ovarian MCs (OMCs) and the relationship between OMCs and early follicular development, and the second chapter examines the genomic factors affecting the appearance of the OMCs.

Contents of this research were published in the following articles.

1. Nakamura, T., Otsuka, S., Ichii, O., Sakata, Y., Nagasaki, K., Hashimoto, Y. and Kon, Y. 2013. Relationship between numerous mast cells and early follicular development in neonatal MRL/MpJ mouse ovaries. PLOS ONE 8:e77246
2. Nakamura, T., Sakata, Y., Otsuka-Kanazawa, S., Ichii, O., Chihara, M., Nagasaki, K., Namiki, Y. and Kon, Y. 2014. Genomic analysis of the appearance of ovarian mast cells in neonatal MRL/MpJ mice. PLOS ONE 9: e100617

Chapter 1

Relationship between numerous mast cells and early follicular development in neonatal MRL/MpJ mouse ovaries

Introduction

MCs reside in most tissues and act as sentinel cells in both innate and adaptive immunity (Galli et al. 2005ab). MCs also contribute to the pathogenesis of cancer, obesity, and diabetes as well as to immunological processes such as allergy and autoimmunity (Coussens et al. 1999; Secor et al. 2000; Robbie-Ryan and Brown 2002; Liu et al. 2009). In rodents, MCs are classified into 2 distinct subpopulations, namely, connective tissue MCs (CTMCs) and mucosal MCs (MMCs). These cell types are distinguished by their staining characteristics, size of cytoplasmic granule, T cell dependency, and expression of MC proteases and inflammatory mediators (Welle 1997). Briefly, mouse CTMCs express MC protease (Mcpt) 4, chymase 1 (Cma1), tryptase beta 2 (Tpsb2), tryptase alpha/beta 1 (Tpsab1), and carboxypeptidase A3 (Cpa3), but lack the MMC markers Mcpt1 and Mcpt2.

In several species including human, the reproductive organs of adult females have different immune cells (Gaytán et al. 1991; Norman and Brännström 1994; Cavender and Murdoch 1988). MCs are also present in the reproductive organs, and the number of MCs varies over the estrous cycle, suggesting an important role of MCs in reproductive function under the control of steroid hormones (Brännström et al. 1993; Woidacki et al. 2013). Furthermore, the appearance of MCs before sexual maturation has been shown in the ovaries of neonatal mice (Skalko et al. 1968). Although it has also been reported that a few MCs are present in the neonatal ovaries of C57BL/6N mice, the functional relationship between MCs and the perinatal ovary is unclear (Kerr et al. 2006).

MRL/MpJ mice have some unique characteristics in the reproductive organs as

shown in preface section. In this chapter, the author found that MRL/MpJ mice possessed a greater abundance of MCs in the neonatal ovaries than other mouse strains. Furthermore, the author determined that the OMCs were mainly CTMCs and were in direct contact with the developing oocytes. The number of MCs had a correlation to the number of developing oocytes. These findings suggest that the appearance of MCs in the neonatal ovary is a unique phenotype of MRL/MpJ mice and that OMCs play a role in oocyte selection of early follicular development in MRL/MpJ mice.

Materials and Methods

Ethical statement

This study was approved by the Institutional Animal Care and Use Committee convened at the Graduate School of Veterinary Medicine, Hokkaido University (approval number: 11-0033). The investigators adhered to the Guide for the Care and Use of Laboratory Animals of Hokkaido University, Graduate School of Veterinary Medicine (approved by the Association for the Assessment and Accreditation of Laboratory Animal Care International).

Animals

Outbred (ICR) and inbred (AKR, C57BL/6N, BALB/c, CBA, C3H/He, DBA/1, DBA/2, NZB, NZW, and MRL/MpJ) mouse strains were used in this chapter. Eight- to ten-week-old male and female mice purchased from Japan SLC (Shizuoka, Japan) were maintained with free access to food and water. Timed mating was established by housing females with males overnight. At noon of the following day, females were checked for the presence of vaginal plugs, and the embryos were recorded as embryonic day 0.5 (E0.5). The female MRL/MpJ and C57BL/6N mice were examined from E15.5 to postnatal day 14 (P14). In addition, the male MRL/MpJ and C57BL/6N mice, and the females of the other strains were obtained at P0 to assess strain differences.

Light microscopy

The liver, kidney, heart, spleen, skin, and testis or ovary from each mouse were

fixed with 4% paraformaldehyde overnight, embedded in paraffin, cut into 1.5- to 3-μm-thick sections, and stained with hematoxylin and eosin (H&E) or toluidine blue (TB).

For histoplanimetric analysis, the sections were stained with 1% TB in 70% ethanol for 30 min, and the number of MCs per organ was measured as the MC density (cells/mm^2). In the ovaries, the number of MCs in the area facing the surface epithelium (SE) per organ was also measured as the SEMC density.

Immunohistochemistry

Immunohistochemistry was performed using the Histofine Mousestain kit (Nichirei, Tokyo, Japan) or the Histofine SAB-PO(M) kit (Nichirei) to detect Tpsab1, F4/80, CD3, and B220 as the cell markers for MCs, macrophages, T cells, and B cells, respectively. Each section was deparaffinized using xylene, rehydrated using graded ethanol, and washed with distilled water. Antigen retrieval was performed with 10 mM citrate buffer (pH 6.0) for 20 min at 105°C (Tpsab1 and CD3) or 0.1% pepsin for 5 min at 37°C (F4/80 and B220). The sections were treated with 0.3% hydrogen peroxidase/methanol solution for 30 min and incubated with blocking reagents (Nichirei) for Tpsab1 or normal goat serum for the other proteins. The sections were incubated at 4°C overnight with mouse anti-Tpsab1 antibody (1:200; Abcam, Cambridge, UK), rat anti-F4/80 antibody (1:100; Cedarlane, Ontario, Canada), rabbit anti-CD3 antibody (1:200; Nichirei), or rat anti-B220 antibody (1:1600, Cedarlane). The Tpsab1 sections were then treated with Histofine Simple Stain MAX-PO(M) (Nichirei)

for 30 min. The other sections were treated with goat biotinylated anti-rabbit IgG antibody (Nichirei) for CD3 or goat biotinylated anti-rat IgG antibody (1:100; Life Technologies, Carlsbad, USA) for F4/80 and B220 for 30 min and then incubated with streptavidin-peroxidase (Nichirei) for 30 min. The immunopositive reactions were developed using a 3,3′-diaminobenzidine-H_2O_2 solution. The sections were also counterstained with hematoxylin.

RT-PCR and quantitative real-time PCR

Total RNA from the ovaries of MRL/MpJ and C57BL/6N mice at P0 was purified using TRIzol reagent (Life Technologies) and treated with DNase (Nippon Gene, Tokyo, Japan). Complementary DNA (cDNA) was synthesized from the RNA using ReverTra Ace (Toyobo, Osaka, Japan) and random primers (Promega, Madison, USA). Each cDNA, adjusted to 1.0 μg/μL, was used for PCR with Go Taq (Promega) and the gene-specific primer pairs shown in Table 1-1. The amplified samples were electrophoresed using 1% agarose gel containing RedSafe (iNtRON Biotechnology, Kyungki-do, Korea) and photographed using an ultraviolet lamp. Quantitative real-time PCR (qPCR) analysis was performed using Brilliant III Ultra Fast SYBR Green QPCR Master Mix (Agilent, Santa Clara, USA) and a real-time thermal cycler (MX 3000P; Stratagene, Milano, Italy).

In situ hybridization

The complementary RNA probes for *Mcpt2* and *Tpsb2* were synthesized in the

presence of digoxigenin-labeled UTP using a DIG RNA labeling kit (Roche Diagnostics, Mannheim, Germany) to detect MMCs and CTMCs, respectively. Table 1-1 shows the primer pairs for each probe synthesis. Deparaffinized sections of the ovaries were treated with proteinase K and then incubated with hybridization buffer containing 40% formamide, 10 mM Tris-HCl (pH 7.6), 200 μg/mL RNA, 100 μg/mL DNA, Denhardt's solution (Sigma-Aldrich, St. Louis, USA), 10% dextran sulfate, 600 mM NaCl, 0.25% SDS, and 1 mM EDTA (pH 8.0) for pre-hybridization. For hybridization, each section was incubated overnight with the sense or antisense RNA probe (final concentration: 0.3 μg/mL) in hybridization buffer at 58°C. After washing with saline sodium citrate buffer, the sections were incubated with sheep anti-digoxigenin Fab fragments conjugated to alkaline phosphatase (1:2000; Nucleic Acid Detection kit; Roche Diagnostics) for 6 h at room temperature. The signal was detected by incubating the sections with a color substrate solution (Roche Diagnostics) in a dark room overnight at room temperature. The sections were counterstained with nuclear fast red.

Immunofluorescence

The deparaffinized sections were treated with 10 mM citrate buffer (pH 6.0) for 20 min at 105°C, treated with normal donkey serum, and incubated with mouse anti-Tpsab1 antibody (1:200) and rabbit anti-DEAD (Asp-Glu-Ala-Asp) box polypeptide 4 (DDX4) antibody (1:200; Abcam) for 3 h at room temperature or with mouse anti-Tpsab1 antibody (1:200) and rabbit anti-tumor necrosis factor-α (TNF-α)

antibody (1:500; AbD Serotec, Oxfordshire, UK) at 4°C overnight. The sections were then incubated with Alexa Fluor 488-labeled donkey anti-mouse IgG and Alexa Fluor 594-labeled donkey anti-rabbit IgG secondary antibody (1:500; Life Technologies) for 30 min, followed by Hoechst33342 (1:200; Dojindo, Kumamoto, Japan) for 30 min. The immunofluorescence signals were examined by confocal microscopy.

For histoplanimetry, the number of Tpsab1-positive MCs contacting DDX4-positive oocytes per ovary was calculated as the density of MCs contacting oocytes. Furthermore, the number of Tpsab1-positive MCs making contact with DDX4-positive oocytes per total number of Tpsab1-positive MCs was calculated as the ratio of MCs contacting oocytes. In addition, to evaluate early follicular development in mice, the numbers of DDX4-positive oocytes and the number of oocytes contacting Tpsab1-positive MCs were counted at each oocyte developmental stage. Briefly, the developmental stages of oocytes were categorized into 3 phases according to the morphology of the oocytes and follicles as follows: 1) nest, several oocytes form cluster; 2) primordial follicle, oocytes are surrounded by simple squamous epithelium; 3) primary follicle, oocytes are surrounded by simple cuboidal epithelium. Intermediate follicles with a single granulosa layer that consisted of both flattened and cuboidal cells were scored as primary follicles.

Electron microscopy

The ovaries of MRL/MpJ and C57BL/6N mice at P0 were immediately fixed with 3% glutaraldehyde in 0.1 M cacodylate buffer (pH 7.3) at 4°C for 4 h. The ovaries were

then post-fixed with 1% osmium tetroxide in 0.1 M cacodylate buffer at room temperature for 2 h, dehydrated with graded alcohol, and embedded in Quetol 812 (Nissin EM, Tokyo, Japan). Ultrathin sections were then stained with uranyl acetate and lead citrate and were observed using a transmission electron microscope.

Statistical analysis

The results were expressed as mean ± SEM values and were analyzed using nonparametric methods. The Mann-Whitney *U* test was used to compare 2 groups. The Kruskal-Wallis test was used to compare 3 or more groups, and multiple comparisons were performed using Scheffé's method. The correlation between 2 groups was analyzed by Pearson's correlation test.

Results

The appearance of OMCs in neonatal MRL/MpJ mice

At P0, TB staining revealed that the MRL/MpJ mouse ovaries contained numerous metachromatic cells (Fig. 1-1A); these cells also had Tpsab1-positive granules in their cytoplasm (Fig. 1-1B). These results clearly demonstrated that the ovaries of MRL/MpJ mice contained MCs. The MCs in MRL/MpJ mice mainly localized to the ovarian cortex rather than to the medulla, and especially accumulated beneath the SE (Fig. 1-1A, B). In contrast, C57BL/6N mice had few MCs in either the ovarian cortex or the medulla (Fig. 1-1C, D). Ultrastructural analysis revealed that the OMCs had pseudopods on the cell surface and segmented or non-segmented nuclei in both strains (Fig. 1-1E, F). In the cytoplasm, the OMCs contained numerous large electron dense granules in MRL/MpJ mice (Fig. 1-1E), but those in C57BL/6N mice had relatively few and small granules (Fig. 1-1F) in accordance with the observations made by TB staining and Tpsab1 immunohistochemistry. To investigate the appearance of the MCs, the MC density in the TB-stained ovary sections was calculated from E15.5 to P14. In MRL/MpJ mice, the OMCs were already observed from E15.5; and the OMC density significantly increased at E17.5, peaked at P0, and gradually decreased from P0 to P14 (Fig. 1-1G). Similar results were observed in the SEMC density. In particular, MRL/MpJ mice showed 40-fold higher values than C57BL/6N mice at P0 (Fig. 1-1H).

Immune cells such as macrophages and lymphocytes were rarely observed in the ovary sections of MRL/MpJ and C57BL/6N mice at P0 (Fig. 1-2A–D). In addition, H&E staining showed that neutrophils and eosinophils were not present in the ovaries of

either strain (Fig. 1-2D).

To examine whether numerous MCs were present in other organs, the MC densities in the liver, kidney, heart, spleen, skin, and testis were also analyzed in MRL/MpJ and C57BL/6N mice at P0 (Table 1-2). MRL/MpJ mice had higher numbers of MCs than C57BL/6N mice in all organs examined, but significant differences were only found in the female skin and ovaries and in the male liver and kidney. Interestingly, although MRL/MpJ mice had numerous MCs in the ovary, only a few MCs were present in the testis. Thus, the author confirmed that the appearance of numerous MCs was an ovary-specific characteristic in neonatal MRL/MpJ mice.

Strain-specific differences in the appearance of OMCs in neonatal mice

To investigate whether the appearance of numerous OMCs was a strain-specific phenotype of MRL/MpJ mice, the OMC density was compared among 11 mouse strains at P0. As shown in Figure 1-3, MRL/MpJ mice had the greatest OMC density among all the examined strains (Fig. 1-3A). Comparatively, ICR, CBA, C3H/He, AKR, NZB, C57BL/6N, and autoimmune-prone NZB mice possessed low MC densities (Fig. 1-3A and B). Interestingly, the ancestral strains of the MRL/MpJ mouse C3H/He, AKR, and C57BL/6N had significantly lower densities than MRL/MpJ mice (Fig. 1-3A). In addition, the MC densities of DBA/2, NZW, BALB/c, and DBA/1 mice were approximately half the value observed in MRL/MpJ mice (Fig. 1-3A); the MCs in these strains tended to appear in the cortex, but not beneath the ovarian SE, which was distinct from the localization in MRL/MpJ mice (Fig. 1-3C). Therefore, the appearance of

numerous MCs and their localization beneath the SE were strain-specific phenotypes in the ovaries of neonatal MRL/MpJ mice.

MC types in the ovaries of neonatal MRL/MpJ mice

To determine the MC type in the ovaries of neonatal MRL/MpJ mice, the expression of MMC markers (*Mcpt1* and *Mcpt2*) and CTMC markers (*Mcpt4*, *Cma1*, *Tpsb2*, *Tpsab1*, and *Cpa3*) was examined by RT-PCR at P0 (Fig. 1-4A). Weak *Mcpt2* expression was detected in the ovaries of MRL/MpJ and C57BL/6N mice, and the band intensity of *Mcpt2* in MRL/MpJ mice was slightly stronger than that in C57BL/6N mice (Fig. 1-4A). No *Mcpt1* expression was detected in the ovaries of either strain. All the examined CTMC markers were detected in the ovaries of both strains. Although the band intensities of *Mcpt4* and *Cma1* in C57BL/6N and MRL/MpJ mice were similar, the *Tpsb2*, *Tpsab1*, and *Cpa3* bands were stronger in MRL/MpJ mice than in C57BL/6N mice (Fig. 1-4A). The product size of *Tpsab1* differed between C57BL/6N and MRL/MpJ mice because C57BL/6N mice have a 98-nucleotide deletion due to the point mutation at the exon 2/intron 2 splice site (Hunt et al. 1996).

Furthermore, the author used *in situ* hybridization to examine the mRNA expression of an MMC marker (*Mcpt2*) and CTMC marker (*Tpsb2*) in the ovaries of MRL/MpJ and C57BL/6N mice at P0. *Mcpt2* mRNA was detected only in the ovaries of MRL/MpJ mice (Fig. 1-4B), and the *Mcpt2*-positive cells localized beneath the ovarian SE. However, no positive reaction was detected in C57BL/6N mice (Fig. 1-4D). Comparatively, *Tpsb2* mRNA was detected in the ovaries of both strains, but the

Tpsb2-positive cells were more abundant in MRL/MpJ mice, especially beneath the SE, than in C57BL/6N mice (Fig. 1-4C, E). Consequently, the numerous MCs in the ovary of neonatal MRL/MpJ mice were considered CTMCs rather than MMCs.

The relationship between OMCs and oocytes

To investigate the relationship between OMCs and oocytes, the expression of the MC marker Tpsab1 and oocyte marker DDX4 was detected by immunofluorescence at P0 in MRL/MpJ, DBA/2, and C57BL/6N mice, which had high, middle, and low OMC densities, respectively (Fig. 1-3A). The DDX4-positive oocytes localized to the ovarian cortex and accumulated beneath the SE in MRL/MpJ, DBA/2, and C57BL/6N mice (Fig. 1-5A–C). Interestingly, some Tpsab1-positive MCs were observed beside or within the cluster of DDX4-positive oocytes, and MCs showed degranulated features in MRL/MpJ (Fig. 1-5D) and DBA/2 mice (Fig. 1-5E). MCs have various chemical mediators, such as TNF-α, whose levels increase with the maturation of MCs during fetal development (Wulff et al. 2012). In the MRL/MpJ mouse ovary, the TNF-α signal overlapped that of Tpsab1, indicating the OMCs produced TNF-α (Fig. 1-5F).

In the neonatal mouse ovary, clusters of oocytes called nests break into smaller cysts and subsequently form primordial and primary follicles (Pepling and Spradling 2001). Ultrastructural analysis of MRL/MpJ mouse ovaries revealed that some MCs directly contacted several oocytes forming large clusters in nests (Fig. 1-5G). In addition, the cytoplasm of the oocytes was compressed by the MCs (Fig. 1-5H), and some of the oocytes showed deformed or vacuolated structures (Fig. 1-5I).

To quantify the relationship between MCs and oocytes, the density of MCs contacting oocytes (Fig. 1-5J) and the ratio of MCs contacting oocytes (Fig. 1-5K) were evaluated. The density of MCs contacting oocytes was highest in MRL/MpJ mice, and the values obtained from MRL/MpJ and DBA/2 mice were significantly higher than those from C57BL/6N mice (Fig. 1-5J). The ratio of MCs contacting oocytes was also significantly higher in MRL/MpJ and DBA/2 mice than in C57BL/6N mice (Fig. 1-5K). Next, the author categorized the oocytes in contact with the MCs into 3 follicle developmental stages, nest, primordial follicles, and primary follicles, and compared the numbers among the 3 strains. The number of oocytes contacting MCs was highest in MRL/MpJ mice, whereas only a few oocytes contacted MCs in C57BL/6N mice (Fig. 1-5L). In MRL/MpJ and DBA/2 mice, most of the oocytes contacting the MCs formed the nest (Fig. 1-5L).

To investigate the functional relationship between the appearance of OMCs and early follicular development in neonatal mice, the follicle developmental stages were compared among MRL/MpJ, DBA/2, and C57BL/6N mice. In all mice examined at P0, the oocytes just beneath the SE formed nests, whereas some oocytes in the deep cortex were enclosed by follicular epithelial cells (Fig. 1-6A–C). In all mice, most of the follicular epithelial cells were squamous, but some were cuboidal in MRL/MpJ and DBA/2 mice. To confirm these observations, the oocyte density was measured in every follicle developmental stage at P0 (Fig. 1-6D–F). The density of nest-stage oocytes was the highest in all follicle stages (Fig. 1-6D, compare the y-axes of Fig. 1-6E, F), and MRL/MpJ mice showed a significantly lower value when compared with DBA/2 and

C57BL/6N mice (Fig. 1-6D). There was no significant strain difference in the density of the primordial follicle (Fig. 1-6E). On the other hand, the density of the primary follicle was significantly higher in MRL/MpJ mice than in C57BL/6N mice (Fig. 1-6F). In MRL/MpJ mice at P0, the density of OMCs significantly and positively correlated with the density of nest-stage oocytes, but not with the density of the primordial follicle (Fig. 1-6G, H). The density of the primary follicle tended to negatively correlate with the density of MCs (Fig. 1-6I). In Fig. 1-6J, the expression of several genes relating to early follicular development was compared between MRL/MpJ and C57BL/6N mice. In MRL/MpJ mice, the expression of *Testis-expressed gene 101* (*Tex101*) was significantly lower, while the expression of *Bone morphogenetic protein 15* (*Bmp15*), *Growth differentiation factor 9* (*Gdf9*), *Zona pellucida glycoprotein 1* (*Zp1*), *Zp2*, and *Zp3* was significantly higher (Fig. 1-6J). Furthermore, the expression of *Tpsb2* derived from OMCs showed a significant positive correlation with the expression of *Tex101*, expressed in nest-stage oocytes, and showed a trend of negative correlation with the expression of *Zp3*, expressed in the primary follicle (Epifano et al. 1995; Takayama et al. 2005) (Fig. 1-4B, 1-6K, L).

Discussion

Abundant MCs in the ovary of neonatal MRL/MpJ mice

MCs in neonatal ovaries were first reported in ICR mice (Skalko et al. 1968). The MCs were present in the hilus of the ovary, the mesovarium, and ovarian bursa, and were most abundant at P0, with numbers decreasing during the first postnatal week. A few MCs have also been reported in the ovaries of neonatal C57BL/6N mice (Kerr et al. 2006). In this chapter, the author demonstrated that not only ICR and C57BL/6N mice, but also other strains possessed OMCs at the neonatal stage. In the neonatal stage, MRL/MpJ mice had the highest OMC density, and the OMCs principally localized beneath the SE, which was distinct from the other strains. Interestingly, the analysis of MCs in various other organs suggested that the appearance of numerous MCs was an ovary-specific phenotype in neonatal MRL/MpJ mice. Therefore, the results demonstrate for the first time that the appearance and localization of OMCs is dependent on the mouse strain. Specifically, the abundance of OMCs beneath the SE is a novel and unique phenotype of neonatal MRL/MpJ mice.

The characteristics of OMCs in neonatal MRL/MpJ mice

Although basophils have metachromatic granules and mono- and multi-globular nuclei similar to MCs, basophils do not express MC-specific proteases (Gurish et al. 1997; Ugajin et al. 2009). In this chapter, the metachromatic cells in the TB-stained ovary of neonatal MRL/MpJ mice were immunopositive for Tpsab1, an MC-specific protease. Furthermore, immune cells other than MCs, such as T cells, B cells,

macrophages, neutrophils, and eosinophils, were rarely observed in the ovaries of neonatal MRL/MpJ mice. These results indicate that MCs are the only immune cells abundantly present in the ovary of neonatal MRL/MpJ mice. Furthermore, electron microscopy results demonstrated that the OMCs in neonatal MRL/MpJ mice contained more granules than those in C57BL/6N mice. Because the size and number of cytoplasmic granules increase as MCs mature during fetal development (Gurish et al. 1997; Wulff et al. 2012), the ultrastructural characteristics of the MCs in MRL/MpJ and C57BL/6N mice suggest mature and immature features, respectively.

All examined CTMC markers were detected in the ovaries of neonatal MRL/MpJ and C57BL/6N mice. Interestingly, the expression of *Tpsb2* and *Tpsab1* was stronger in MRL/MpJ mice than in C57BL/6N mice. Furthermore, *Tpsb2* (CTMC marker gene)-expressing cells were more abundant beneath the ovarian SE in MRL/MpJ mice than in C57BL/6N mice. These results demonstrate that the majority of OMCs identified are CTMCs. In addition, a small number of *Mcpt2* (MMC marker gene)-expressing cells were detected beneath the ovarian SE from neonatal MRL/MpJ mice, but not from neonatal C57BL/6N mice. The expression pattern of MC proteases differs across mouse strains and tissues. Briefly, although *Mcpt2* (MMC marker gene) was detected in the ear of WB/ReJ mice, no expression was detected in BALB/c mice (Stevens et al. 1994). Furthermore, CTMCs expressed both CTMC and MMC markers in the trachea and large bronchi of normal mice (Xing et al. 2011). Therefore, these data emphasize that MMC marker-expressing MCs and abundant ovarian CTMCs are unique phenotypes in neonatal MRL/MpJ mice. The author proposes that the mouse strain or ovary-specific

microenvironment mediates the expression of MC-specific protease genes.

The relationship between the appearance of OMCs and early follicular development

In neonatal mouse ovaries, oocytes undergo a process called nest breakdown in which oocytes in the nest break into smaller cysts until a few individual oocytes remain. The individual oocytes are finally surrounded by follicular epithelial cells to form primordial follicles and then develop into primary follicles (Pepling and Spradling 2001). To determine the relationship between MCs and oocytes in the neonatal ovary, the author observed the co-localization of MCs and oocytes with follicular development. In MRL/MpJ and DBA/2 mice, more than 20% of the MCs localized mainly beside oocytes in the nest. Furthermore, the density of nest-stage oocytes and the gene expression of *Tex101* in nest-stage oocytes were significantly lower in MRL/MpJ mice than in C57BL/6N mice. In addition, the density of primary follicles and the expression of genes associated with follicular development (*Bmp15*, *Gdf9*, *Zp1*, *Zp2*, and *Zp3*) were higher in MRL/MpJ mice than in C57BL/6N mice. These findings indicate that MCs tend to localize beside the nest-stage oocyte rather than the primordial or primary follicle and that follicular development occurs earlier in MRL/MpJ than in C57BL/6N mice, which have high and low OMC densities, respectively.

In MRL/MpJ mice at P0, the density of MCs positively correlated with the density of nest-stage oocytes. Similarly, the expression of an MC marker gene had a significant positive correlation with the expression of a marker for nest-stage oocytes. Further, a trend of negative correlation was suggested between the density of MCs and the density

of the primary follicle and between an MC marker gene and a primary follicle marker gene although OMCs did not contact the primary follicle. Importantly, the number of OMCs in MRL/MpJ mice significantly increased at E17.5, before nest breakdown; they were most evident at P0, the time of nest breakdown, and decreased thereafter. Therefore, the results indicate that OMCs increase in accordance with the timing of nest breakdown and decrease with follicular development in neonatal MRL/MpJ mice.

Approximately two-thirds of oocytes die during nest breakdown by several possible mechanisms, including apoptosis and autophagic cell death (Coucouvanis et al. 1993; De Pol et al. 1997; De Felici et al. 2008; Rodrigues et al. 2009). TNF-α, which induces apoptosis and autophagy, plays an important role in the process of germ cell death in fetal/neonatal mice and rats (Marcinkiewicz et al. 2002; Jia et al. 2006; Greenfeld et al. 2007). In addition, MCs can induce endothelial cell apoptosis via TNF-α (Lätti et al. 2003; Heikkila et al. 2008). In fact, OMCs in MRL/MpJ mice expressed TNF-α and directly contacted the degenerative oocytes in the nest at P0. Some of the degenerative oocytes in MRL/MpJ mice exhibited vacuolated cytoplasm, which is typical of autophagy (Lobascio et al. 2007). Therefore, OMCs are closely related to nest breakdown and this process might be regulated by oocytic death via several mediators, such as TNF-α derived from the numerous OMCs. In addition, the increase of the primary follicle in MRL/MpJ mice might be a result of the accelerated nest breakdown.

In conclusion, the author has demonstrated that the appearance of numerous OMCs is strain-dependent. Their abundance, localization, and gene expression are unique in

neonatal MRL/MpJ mice. The author proposes that MCs are involved in the process of early follicular development, especially nest breakdown, which predicts a new function of MCs.

Summary

In the neonatal mouse ovary, clusters of oocytes called nests break into smaller cysts and subsequently form individual follicles. During this period, the author found numerous MCs in the ovary of MRL/MpJ mice and investigated their appearance and morphology with follicular development. In MRL/MpJ mice at postnatal day 0, the appearance of numerous MCs was an ovary-specific phenotype compared to C57BL/6N mice, and the MCs were the only immune cells abundantly present in the ovary. In MRL/MpJ mice, the OMCs were most abundant at postnatal day 0, and tended to localize adjacent to the SE. Among 11 different mouse strains, MRL/MpJ mice possessed the greatest number of OMCs. OMCs were also found in DBA/1, BALB/c, NZW, and DBA/2 mice but rarely in C57BL/6N, NZB, AKR, C3H/He, CBA, and ICR mice. The OMCs expressed CTMC markers, although MCs beneath the SE also expressed a MMC marker in MRL/MpJ mice. Some OMCs migrated into the oocyte nests and directly contacted the compressed and degenerated oocytes. In MRL/MpJ mice, the number of oocytes in the nest was significantly lower than in the other strains, and the number of oocytes showed a positive correlation with the number of OMCs. The gene expression of a MC marker also correlated with the expression of an oocyte nest marker, suggesting a link between the appearance of OMCs and early follicular development. Furthermore, the expression of follicle developmental markers was significantly higher in MRL/MpJ mice than in C57BL/6N mice. These results indicate that the appearance of OMCs is a unique phenotype of neonatal MRL/MpJ mice and that OMCs participate in nest breakdown, accelerating early follicular development.

Tables and Figures

Table 1-1. Summary of the specific gene primers used in this chapter.

Gene	Forward Primer (5′–3′)	Reverse Primer (5′–3′)	Product size	Accession #
Mcpt1	AAACAGTCATAAATGGCAAG	GGGAACAAACCATCATCAC	237 bp	NM_008570
Mcpt2	GTGATGACTGCTGCACACTG	CTTGAAGAGTCTGACTCAGG	595 bp	NM_008571
Mcpt4	CCTTACATGGCCCATCT	CTTCCCCGGCTTGATA	327 bp	NM_010779
Cpa1	ACCTCTGCTGTGTGCTGGGATAG	TTTGCAGTTGACAATCTGGGTCTT	333 bp	NM_010780
Tpsb2	CTCTCTCATCCACCCACAGT	TGTAGATGCCAGGCTTGTTG	590 bp	NM_010781
	CGACATTGATAATGACGAGCCTC	ACAGGCTGTTTTCCACAATGG	80 bp	
Tpsab1	AGTGGCCAAGCCATTAGAG	TCTGGCTCACAGTCATCAGG	449 (351) bp	NM_031187
Cpa3	ACACAGGATCGAATGTGGAG	TAATGCAGGACTTCATGAGC	690 bp	NM_007753
Tex101	ATCTTTCTTCTAATCGCCTCACG	GCTCAGCCTTTGAAGTCCAGT	121 bp	NM_019981
Bmp15	CGATTGGAGCGAAAATGGTG	CCAGAGCTTCTGCTGAATAC	320 bp	NM_009757
Gdf9	ACGTATGCTACCAAAGAGGG	CAGAGTGTATAGCAAGACCG	204 bp	NM_008110
Zp1	CCCTGAGATTGGGTCAGCG	AGAGCAGTTATTCACCTCAAACC	164 bp	NM_009580
Zp2	GCACTTATGCTCTGGACTTGG	TGCTTGAATAGCTGGACAGAA	167 bp	NM_011775
Zp3	CCTCAGGACTAACCGTGTGGA	CCATCAGGCGAAGAGAGAAAG	149 bp	NM_011776
Actb	TGTTACCAACTGGGACGACA	GGGGTGTTGAAGGTCTCAAA	165 bp	NM_007393

For *Tpsab1*, C57BL/6 mice had a smaller gene product size than MRL/MpJ mice because of a 98-nucleotide deletion due to a point mutation at the exon 2/intron 2 splice site (Hunt et al. 1996).

Table 1-2. Mast cell density in various organs at postnatal day 0.

		Liver	Kidney	Heart	Spleen	Skin	Ovary/Testis
Female	MRL/MpJ	0.7 ± 0.1	2.9 ± 0.9	8.7 ± 1.1	575.8 ± 82.1	555.4 ± 19.2**	461.7 ± 79.8**
	C57BL/6N	0.3 ± 0.1	1.0 ± 0.3	8.2 ± 0.6	372.6 ± 67.3	361.1 ± 25.0	59.2 ± 10.4
Male	MRL/MpJ	1.1 ± 0.3*	2.8 ± 0.2*	6.6 ± 1.1	658.4 ± 72.0	604.9 ± 66.9	4.1 ± 2.1
	C57BL/6N	0.2 ± 0.2	0.2 ± 0.1	7.0 ± 1.0	356.1 ± 6.0	456.8 ± 32.2	0.0 ± 0.0

Units: number of mast cells/mm^2. Data represent the mean ± SEM (n = 4–6 in each group). Significant differences were analyzed using the Mann-Whitney *U* test in the same sex. * $P < 0.05$, ** $P < 0.01$.

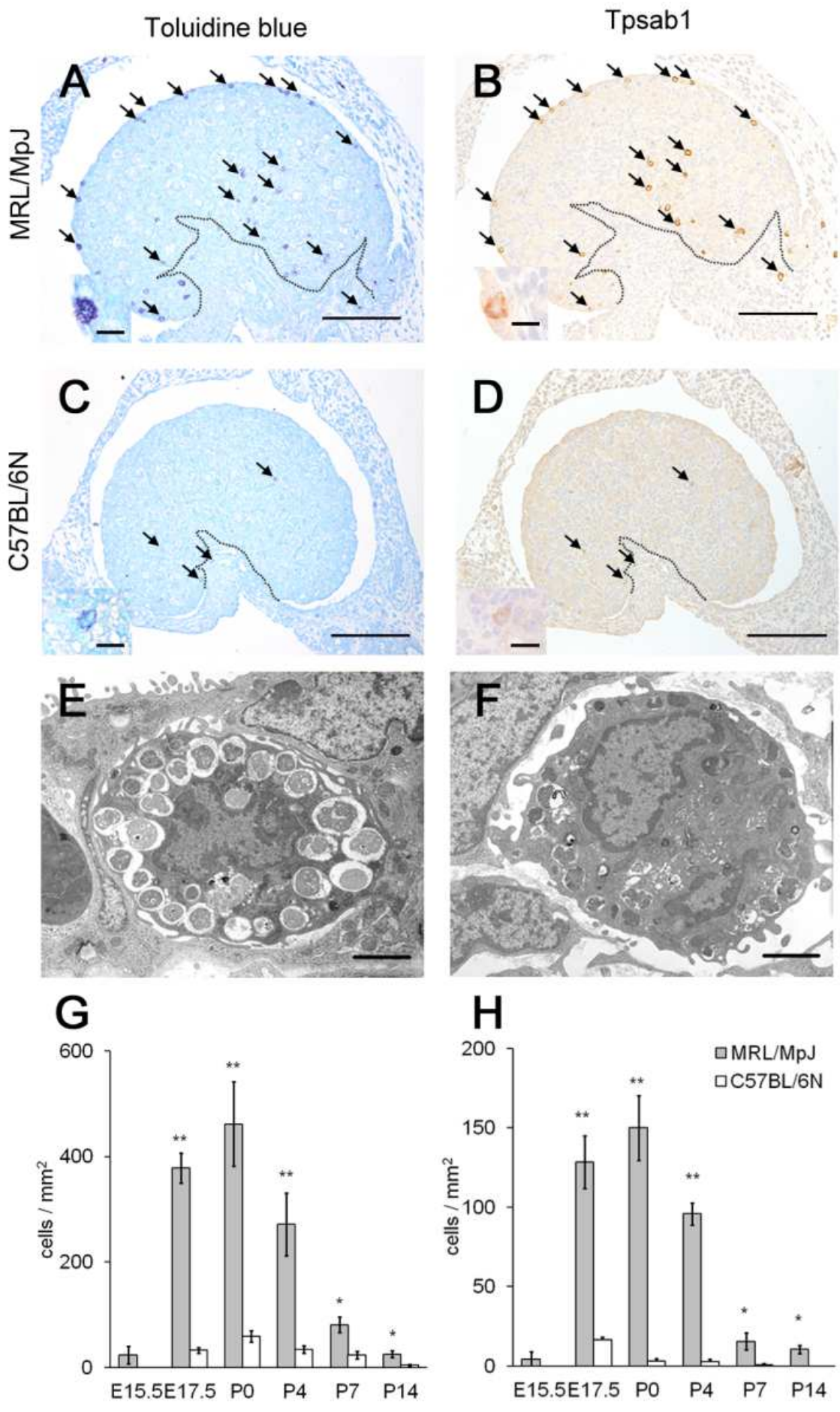
Toluidine blue
Tpsab1
MRL/MpJ
C57BL/6N
A
B
C
D
E
F
G
H
600
400
200
0
cells / mm2
E15.5
E17.5
P0
P4
P7
P14
MRL/MpJ
C57BL/6N
200
150
100
50
0

Figure 1-1. The appearance of mast cells in the ovaries of neonatal mice.

(A–D) The ovaries of neonatal mice. Serial sections of mouse ovaries at postnatal day 0 were stained with toluidine blue (panels A and C) or immunohistochemistry for the mast cell (MC) marker Tpsab1 (panels B and D). Arrows and insets indicate the same cells. Dotted lines indicate the border between the cortex and medulla of the ovary. Bars in panels: 100 μm. Bars in insets: 10 μm. (E and F) The ultrastructure of MCs in ovaries of MRL/MpJ mice (panel E) and C57BL/6N mice (panel F) at postnatal day 0. Bars: 2 μm. (G and H) MC density in mouse ovaries. The number of metachromatic MCs in the whole area of the ovary (panel G) or in the area facing the ovarian surface epithelium (panel H) was divided by the area of the ovary. Data represent the mean ± SEM (n = 3–6 in each group). Significant differences between MRL/MpJ and C57BL/6N mice were analyzed using the Mann-Whitney *U* test at each time point. *: $P < 0.05$, **: $P < 0.01$.

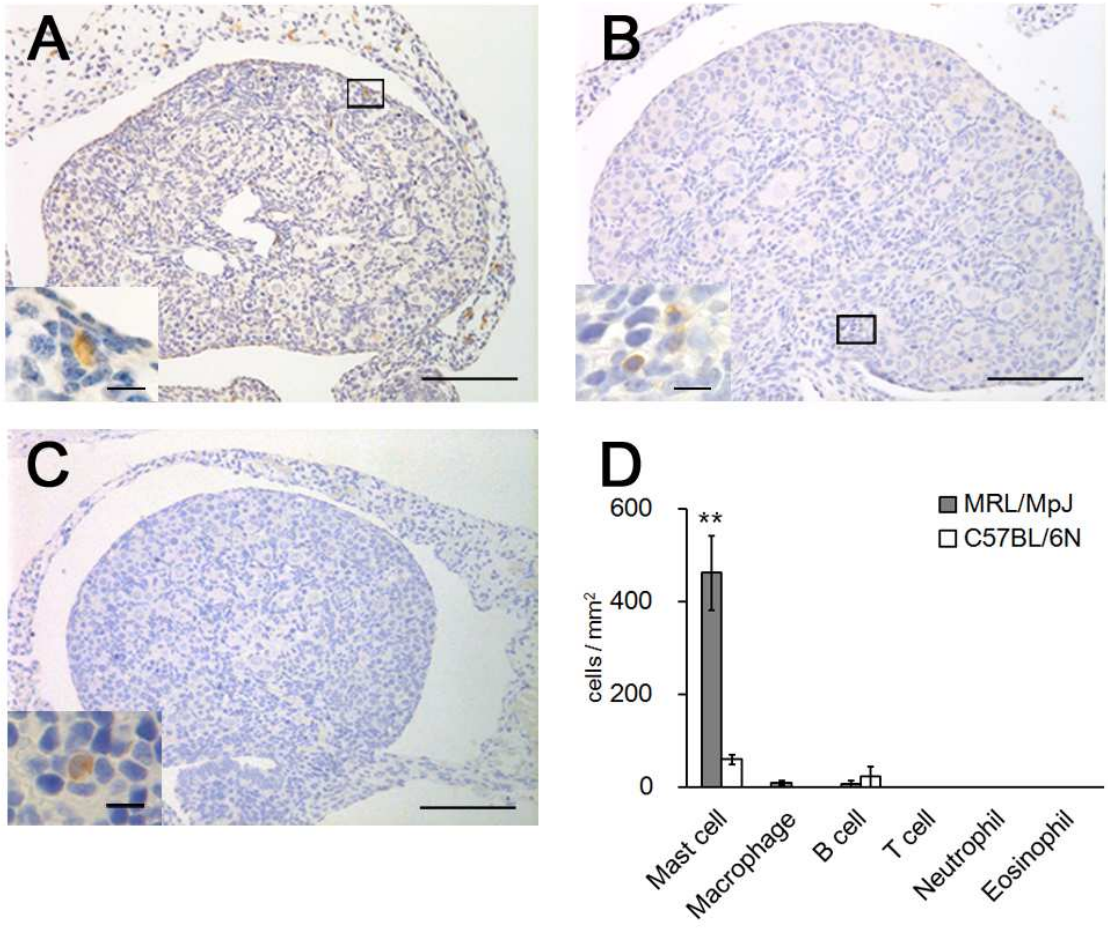

Figure 1-2. The appearance of immune cells in the ovaries of neonatal mice.

(A–C) The ovaries of MRL/MpJ mice at postnatal day 0. Immunohistochemical analysis of F4/80 (macrophage marker, panel A), B220 (B cell marker, panel B), and CD3 (T cell marker, panel C). The insets show a higher magnification of the boxed area in panels A and B. In panel C, the inset shows the spleen section at postnatal day 0 as a positive control. Bars in panels: 100 μm. Bars in insets: 10 μm. (D) Number of immune cells in the ovaries at postnatal day 0. Data represent the mean ± SEM (n = 3–6 in each group). Significant differences were analyzed using the Mann-Whitney *U* test. **: $P < 0.01$.

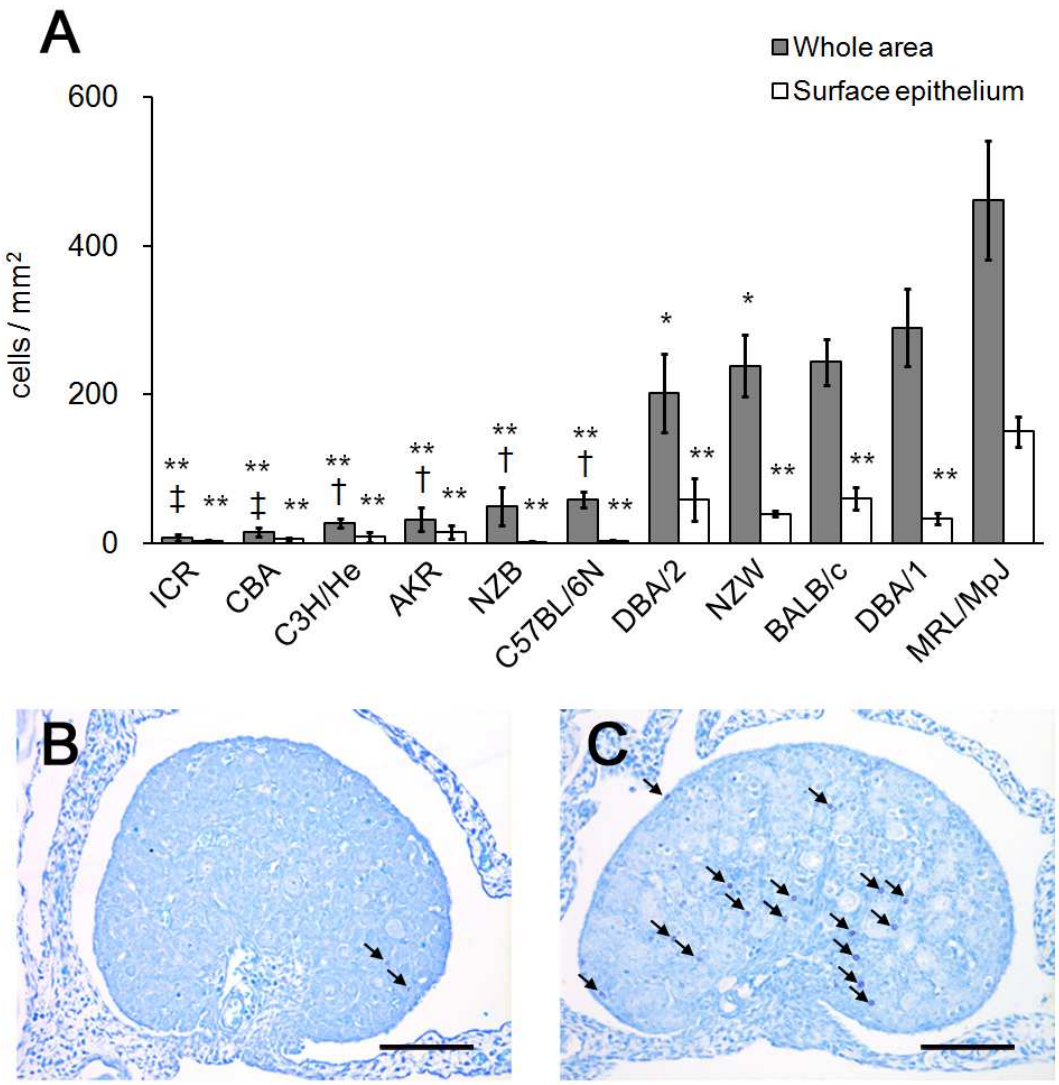

Figure 1-3. Strain differences in the appearance of ovarian mast cells in neonatal mice. (A) Ovarian mast cell (MC) density among 11 mouse strains at postnatal day 0. The number of metachromatic MCs in the whole area of the ovary (gray bars) or in area facing the ovarian surface epithelium (white bars) was divided by the area of the ovary. Data represent the mean ± SEM (n = 4–8 in each group). Significant differences were analyzed using Scheffé's method subsequent to the Kruskal-Wallis test. *: $P < 0.05$, **: $P < 0.01$ vs. MRL/MpJ mice. †: $P < 0.05$, ‡: $P < 0.01$ vs. DBA/1 mice. (B and C) Toluidine blue-stained ovary sections of neonatal CBA mice (panel B) and BALB/c mice (panel C). Arrows indicate the MCs. Bars: 100 μm.

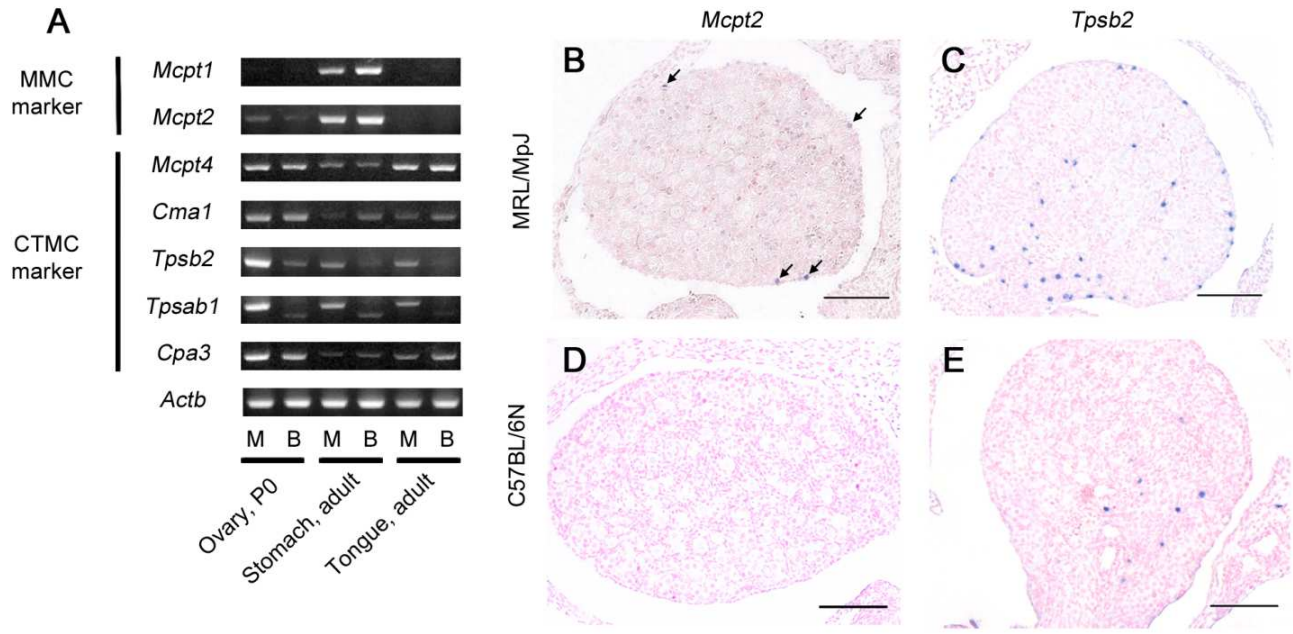

Figure 1-4. Gene expression of mast cell-specific proteases in the ovaries of neonatal mice.

(A) RT-PCR was used to measure the mRNA expression of a mast cell (MC)-specific protease in the mouse ovary at postnatal day 0. Stomach and tongue samples from adult mice were used as positive controls for MMCs and CTMCs, respectively. *Actb* was used as an internal control. M: MRL/MpJ mice. B: C57BL/6N mice. (B–E) *In situ* hybridization of *Mcpt2* and *Tpsb2* in the ovaries at postnatal day 0. *Mcpt2*-positive signals are detected beneath the surface epithelium of the MRL/MpJ mouse ovary (panel B, arrows). No positive signal is observed in the ovaries of C57BL/6N mice (panel D). *Tpsb2*-positive signals are detected in both strains (panels C and E) but are more abundant in MRL/MpJ mice (panel C). Bars: 100 μm.

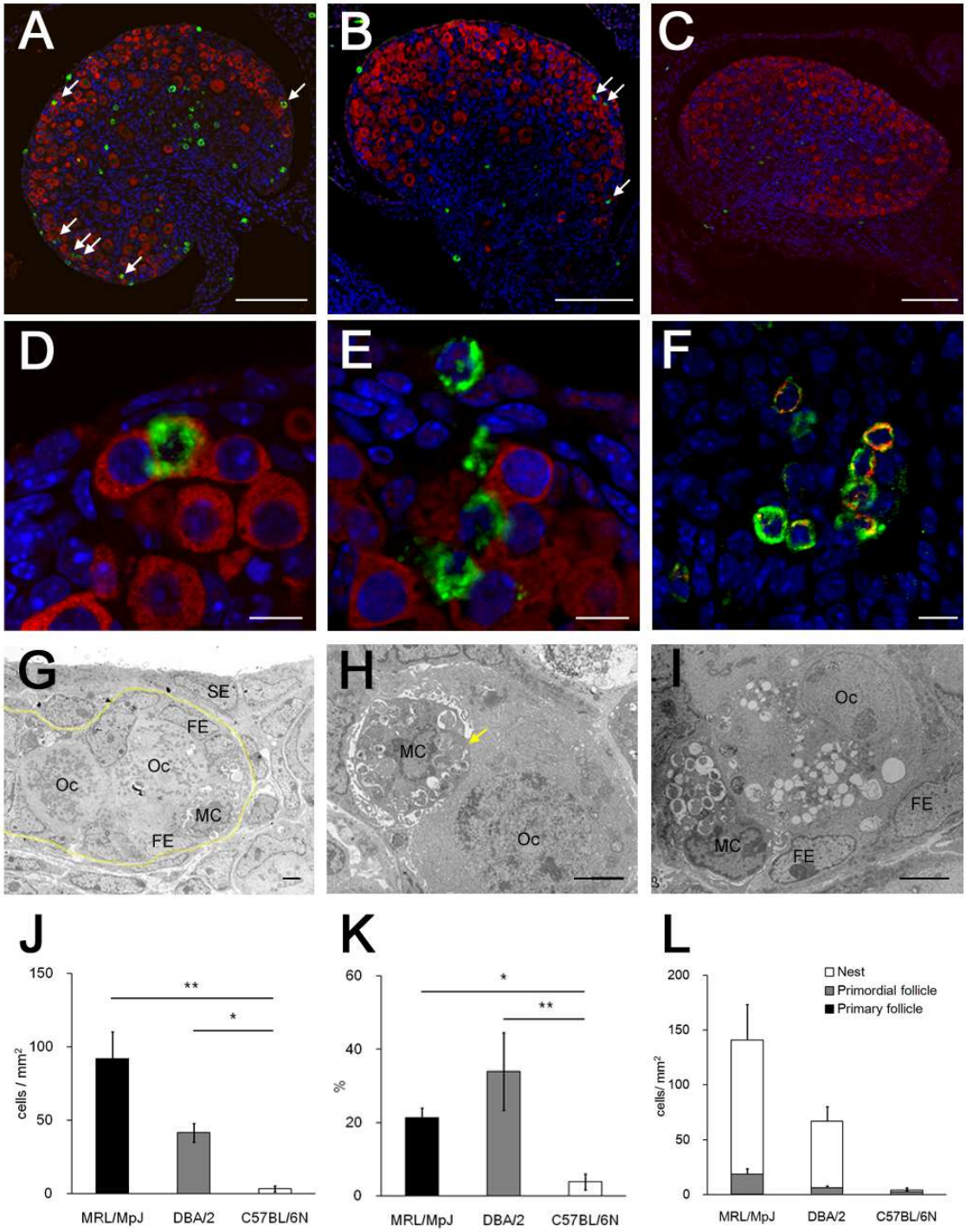
A
B
C
D
E
F
G
SE
FE
Oc
Oc
MC
FE
H
MC
Oc
I
Oc
FE
MC
FE
J
150
100
50
0
cells / mm²
**
*
MRL/MpJ
DBA/2
C57BL/6N
K
60
40
20
0
%
*
**
MRL/MpJ
DBA/2
C57BL/6N
L
200
150
100
50
0
cells/ mm²
Nest
Primordial follicle
Primary follicle
MRL/MpJ
DBA/2
C57BL/6N

Figure 1-5. The relationship between mast cells and oocytes in the ovaries of neonatal mice.

(A–C) The localization of mast cells (MCs) and oocytes (Ocs) in the ovary of MRL/MpJ (panel A), DBA/2 (panel B), and C57BL/6N mice (panel C) at postnatal day 0. Tpsab1 (green) and DDX4 (red) were detected as markers for MCs and Ocs, respectively. Bars: 100 μm. (D and E) Higher magnification of the ovaries from MRL/MpJ (panel D) and DBA/2 mice (panel E). (F) The expression of TNF-α in the ovarian MCs of MRL/MpJ mice at postnatal day 0. TNF-α (red) is expressed in Tpsab1 (green)-positive MCs. Bars: 10 μm. (G–H) Ultrastructure of MCs and Ocs in the ovaries of neonatal MRL/MpJ mice. The nest is surrounded by a yellow dotted line. Arrow indicates the compression of Oc cytoplasm by MCs. FE: follicular epithelial cell. SE: surface epithelial cell. Bars: 2 μm. (J) The total number of MCs contacting Ocs. (K) The ratio of the number of MCs contacting Ocs to the total number of MCs. (L) The number of Ocs contacting MCs. Ocs were categorized according to the developmental stage: nest, primordial follicle, or primary follicle. Data represent the mean ± SEM (n = 4–5 in each group). Significant differences were analyzed using Scheffé's method subsequent to the Kruskal-Wallis test. *: $P < 0.05$, **: $P < 0.01$.

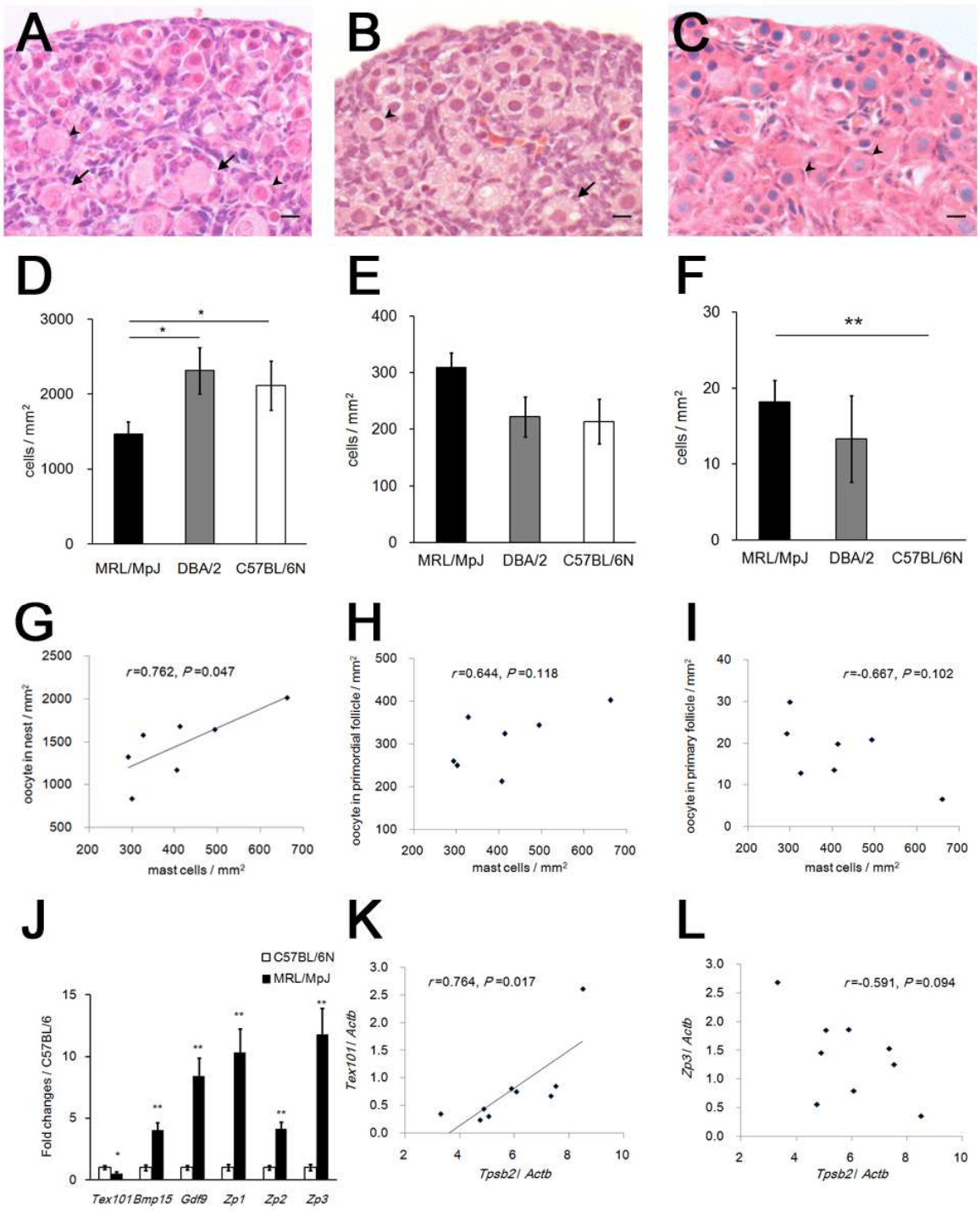
A
B
C
D
cells / mm²
3000
2000
1000
0
*
*
MRL/MpJ
DBA/2
C57BL/6N
E
cells / mm²
400
300
200
100
0
MRL/MpJ
DBA/2
C57BL/6N
F
cells / mm²
30
20
10
0
**
MRL/MpJ
DBA/2
C57BL/6N
G
oocyte in nest / mm²
2500
2000
1500
1000
500
r=0.762, P=0.047
200
300
400
500
600
700
mast cells / mm²
H
oocyte in primordial follicle / mm²
500
400
300
200
100
r=0.644, P=0.118
200
300
400
500
600
700
mast cells / mm²
I
oocyte in primary follicle / mm²
40
30
20
10
0
r=-0.667, P=0.102
200
300
400
500
600
700
mast cells / mm²
J
C57BL/6N
MRL/MpJ
Fold changes / C57BL/6
15
10
5
0
*
**
**
**
**
Tex101
Bmp15
Gdf9
Zp1
Zp2
Zp3
K
Tex101 / Actb
3.0
2.5
2.0
1.5
1.0
0.5
0.0
r=0.764, P=0.017
2
4
6
8
10
Tpsb2 / Actb
L
Zp3 / Actb
3.0
2.5
2.0
1.5
1.0
0.5
0.0
r=-0.591, P=0.094
2
4
6
8
10
Tpsb2 / Actb

Figure 1-6. Early follicular development in the ovary of neonatal mice.

(A–C) Mouse ovaries at postnatal day 0. Sections from MRL/MpJ (panel A), DBA/2 (panel B), and C57BL/6N (panel C) mice were stained using hematoxylin and eosin. Arrowheads indicate primordial follicles. Arrows indicate primary follicles. Bars: 10 μm. (D–F) The number of oocytes in the mouse ovaries at postnatal day 0. DDX4-positive oocytes per ovary area were counted according to 3 developmental stages: nest (panel D), primordial follicle (panel E), and primary follicle (panel F). Data represent the mean ± SEM (n = 4–7 in each group). (G–I) Correlation between the number of mast cells and oocytes in the nest (panel G), primordial follicle (panel H), and primary follicle (panel I) in MRL/MpJ mice at postnatal day 0 (Pearson's correlation test, n = 7). (J) qPCR analyses of *Tex101*, *Bmp15*, *Gdf9*, *Zp1*, *Zp2*, and *Zp3* genes at postnatal day 0. Data represent the mean ± SEM (n = 7–9 in each group). (K and L) Correlation between the gene expression of *Tpsb2* and *Tex101* (panel K) or *Zp3* (panel L) in MRL/MpJ mice at postnatal day 0 (Pearson's correlation test, n = 9). Significant differences were analyzed using Scheffé's method subsequent to the Kruskal-Wallis test (D–F) or Mann-Whitney *U* test (J). *: $P < 0.05$, **: $P < 0.01$.

Chapter 2

Genomic analysis of the appearance of ovarian mast cells in neonatal MRL/MpJ mice

Introduction

MRL/MpJ mice originate from C57BL/6J (0.3%), C3H/HeDi (12.1%), AKR/J (12.6%), and LG/J (75.0%) strains. MRL/MpJ mice, models for autoimmune diseases, show some unique phenotypes related to wound healing and reproductive organs (Theofilopoulos and Dixon 1985; Clark et al. 1998; Kon et al. 1999, 2007; Kon and Endoh 2000, 2001; Nose et al. 2000; Leferovich et al. 2001; Otsuka et al. 2008ab). These phenotypes were closely associated with the genetic background of MRL/MpJ mice, and several susceptibility loci were identified by quantitative trait locus (QTL) analysis (Namiki et al. 2003, 2005; Yu et al. 2005; Lee et al. 2010; Otsuka et al. 2012).

In the Chapter 1, the author clarified that neonatal MRL/MpJ mice possess numerous MCs in the ovary, and the OMCs tended to localize beneath the ovarian SE. These characteristic phenotypes of OMCs were not observed in other inbred strain including C57BL/6N. Therefore, the abundance and the distribution of MCs were considered to be strain-specific phenotypes in the ovaries of neonatal MRL/MpJ mice.

In this chapter, the author tried to clarify the factors affecting the abundance of OMCs and its localization to SE in neonatal MRL/MpJ mice by genetic analysis using the progenies between MRL/MpJ and C57BL6/N mice.

Materials and Methods

Ethical statement

This study was approved by the Institutional Animal Care and Use Committee convened at the Graduate School of Veterinary Medicine, Hokkaido University (approval number: 13-0086). The investigators adhered to the Guide for the Care and Use of Laboratory Animals of Hokkaido University, Graduate School of Veterinary Medicine (approved by the Association for the Assessment and Accreditation of Laboratory Animal Care International).

Animals

MRL/MpJ and C57BL/6N mice were purchased from Japan SLC. Timed mating was established by housing females with males overnight. At noon of the following day, females were checked for the presence of a vaginal plug, and the embryos were recorded as E0.5. C57BL/6N mice were mated with MRL/MpJ mice to produce F1 and F2 progeny. In addition, 200 female N2 backcross progenies (BMM) were generated for QTL analysis by mating female B6MRLF1 (a cross between female C57BL/6N and male MRL/MpJ mice) with male MRL/MpJ mice.

Histological analysis and phenotyping

The TB-stained ovarian sections were prepared as described in Chapter 1. The OMC density and the SEMC density were measured, and SEMC ratio was calculated as the ratio of SEMC to OMC densities.

Artificially delayed parturition model

To delay parturition, pregnant MRL/MpJ and C57BL/6N mice were subcutaneously injected with progesterone (2 mg/head; Sigma-Aldrich) suspended in sesame oil every 24 h from E17.5 to E20.5 (Kokubu et al. 2005). At E21.5 when the parturition was delayed for 2 days, ovaries of fetuses were collected, with those of age-matched P2 mice serving as controls. P0 and P4 ovaries were also examined.

Measurement of plasma sex hormone levels

Heparinized plasma was collected from female fetuses of MRL/MpJ and C57BL/6N mice at E18.5 of normal pregnancy. Plasma estradiol and progesterone were measured by enzyme-linked immunosorbent assay (Cayman Chemical Company, Ann Arbor, USA).

Genotyping

Genomic DNA was prepared from the tail of each BMM mouse using a standard protocol. In total, 94 microsatellite markers identified in the Mouse Genome Informatics database of the Jackson Laboratory (www.informatics.jax.org) were used for a genome-wide scan, with a mean intermarker distance of 10–20 cM, to genotype the C57BL/6N or MRL/MpJ allele (Table 2-1). PCR was performed with GoTaq (Promega) under the following PCR conditions: 2 min at 94°C; 40 cycles of 40 s at 94°C, 30 s at 58°C, and 20 s at 72°C; and 5 min at 72°C. To compare sizes of PCR products, amplified samples were resolved by electrophoresis using agarose 3:1 (2–4%;

AMRESCO, Inc., Solon, USA) which was stained with ethidium bromide and imaged under an ultraviolet lamp.

QTL analysis

To examine susceptibility loci associated with the appearance of OMCs in neonatal MRL/MpJ mice, QTL analysis was performed using 200 BMM mice at P0. For the appearance of MCs in neonatal ovary, OMC density, SEMC density, and SEMC ratio were applied as quantitative traits (QTs). Linkage analyses were performed using the Map Manager QTX20b program (Manly et al. 2001). Thresholds for likelihood ratio statistics (LRS) were determined by genome-wide 1000-permutation test to provide the suggestive, significant, and highly significant levels. In addition, epistatic interactions between pairs of marker loci were also searched using the Map Manager software. The threshold for significant LRS was estimated by a 1000-permutation test.

In silico analysis of single nucleotide polymorphisms

For several genes coded as highly significant QTL, single nucleotide polymorphisms (SNPs) specifically associated with non-synonymous coding polymorphisms were determined in MRL/MpJ- and C57BL/6N-type genomes using the Mouse Phenome Database (MPD) from Jackson Laboratory (http://phenome.jax.org).

Reverse transcription and quantitative real-time PCR

Total RNA from ovaries of P0 MRL/MpJ and C57BL/6N mice was purified,

synthesized to cDNA, and qPCR was performed as described in Chapter 1. Gene-specific primer pairs are listed in Table 2-2.

Statistical analysis

Results are expressed as mean ± SEM and were analyzed using nonparametric methods as described in Chapter 1.

Results

Appearance of OMCs in MRL/MpJ and C57BL/6N mice, and their progeny

To determine the pattern of inheritance, the appearance of OMCs was compared between MRL/MpJ and C57BL/6N mice and their F1 and F2 progeny at P0. Metachromatic MCs were abundant in ovaries of MRL/MpJ mice (Fig. 2-1A), but rarely seen in C57BL/6N ovaries (Fig. 2-1B). OMCs were observed in both direct F1 (MRLB6F1, a cross between female MRL/MpJ and male C57BL/6N mice) and reciprocal F1 (B6MRLF1) at P0 (Fig. 2-1C, D). The F2 progeny (MRLB6F2 and B6MRLF2) also had OMCs at P0 (Fig. 2-1E, F). Although MCs were distributed in the deep layer of the ovarian cortex in MRL/MpJ, F1, and F2 mice, they were more frequently observed beneath the ovarian SE in MRL/MpJ mice than in their F1 and F2 progeny (Fig. 2-1A, C–F).

OMC density was 50-fold higher in MRL/MpJ than in C57BL/6N mice (Fig. 2-1G), while values in F1 and F2 were less than half of that observed in the MRL/MpJ parental strain. These results suggested that the appearance of OMCs was controlled by at least recessive factor. Notably, MRLB6F1 mice had a significantly higher number of OMCs than B6MRLF1 (Fig. 2-1G). In contrast, no differences were observed in OMC density between MRLB6F2 and B6MRLF2. Similar trends were observed for SEMC density (Fig. 2-1H). The SEMC ratio, an index of OMC localization beneath the ovarian SE, was also higher in MRL/MpJ than in C57BL/6N, F1, and F2; however, the ratio was similar between direct and reciprocal F1 progeny (Fig. 2-1I). These results suggest that both parental strains and filial genetic factors affect the abundance of OMCs, but

distribution of MCs beneath the ovarian SE is mainly regulated by filial genetic factors.

Effects of maternal factors on the appearance of OMC

Based on the results of histoplanimetric analyses of F1 progeny, it was supposed that environmental factors during pregnancy affect the abundance of OMCs in perinatal mice. To test this hypothesis, parturition was delayed by injecting pregnant MRL/MpJ and C57BL/6N mice with progesterone, and OMC density was compared between E21.5 fetuses and age-matched P2 pups. In MRL/MpJ mice, MCs were abundant in the ovary at E21.5 (Fig. 2-2A), and these numbers tended to be higher than in P2 ovary of normal parturition (Fig. 2-2B). OMC density in normal parturition mice was highest at P0, and gradually decreased thereafter, but in E21.5 fetuses, the value was higher than in age-matched P2 mice, and comparable to P0 mice of normal parturition (Fig. 2-2C). In contrast, in C57BL/6N mice, OMC density at E21.5 was lower than in P2 controls (Fig. 2-2D). Consistent with the F1 analysis, SEMC ratio did not differ between E21.5 fetuses and age-matched P2 mice in both strains (Fig. 2-2E, F). In mammals, fetuses are exposed to high doses of steroid hormones during late pregnancy, and their hormones affect MC properties in the adult ovary (Zierau et al. 2012). However, neither plasma estradiol nor progesterone levels differed between MRL/MpJ and C57BL/6N mice at E18.5 of normal pregnancy (Fig. 2-2G, H).

QTL analysis of OMC appearance in neonatal BMM mice

To identify the genetic loci controlling the appearance of OMCs in neonatal

MRL/MpJ mice, a genome-wide QTL analysis was performed using 200 BMM mice at P0. Since both OMC abundance and their distribution beneath the ovarian SE were unique phenotypes of MRL/MpJ mice, OMC density, SEMC density, and SEMC ratio were measured as QTs. All QTs had gradient distributions, suggesting a polygenic pattern of inheritance (Fig. 2-3A–C). SEMC density was positively correlated with both OMC density and SEMC ratio (Fig. 2-3D, E), but there was no correlation between these latter traits (Fig. 2-3F), suggesting that OMC density and SEMC ratio were independent QTs corresponding to the number and distribution of OMCs, respectively, while SEMC density arose from the combination of these two traits.

Using OMC density as a trait, suggestive QTL were mapped to C57BL/6N-type *D4Mit42* (LRS = 7.0, 82.64 cM) (Fig. 2-4A, Table 2-3). In addition, a significant locus was mapped to MRL/MpJ-type *D8Mit343–D8Mit312* (LRS > 12.0, 39.33–47.12 cM), with one highly significant peak on *D8Mit248–D8Mit312* (LRS > 19.0, 44.99–47.12 cM) (Fig. 2-4B, G, Table 2-3).

For SEMC density, suggestive loci were mapped to MRL/MpJ-type *D2Mit340* (LRS = 8.4, 73.59 cM), MRL/MpJ-type *D13Mit17* (LRS = 6.5, 7.73 cM), and C57BL/6N-type *D14Mit11-D14Mit141* (LRS > 6.3, 6.33-24.28 cM) (Fig. 2-4C, Table 2-3). Bimodal, significant peaks were detected on Chr 8 (Fig. 2-4D). Significant QTL were mapped to MRL/MpJ-type *D8Mit8–D8Mit89* (LRS > 12.1, 32.30–62.93 cM), with one highly significant peak on *D8Mit343–D8Mit312* (LRS > 20.1, 39.33–47.12 cM) overlapping the highly significant locus for OMC density, and the other peak on *D8Mit86–D8Mit89* (LRS > 12.1, 56.18–62.93 cM) (Fig. 2-4D, H, I, Table 2-3). These

two significant QTL were designated as *mast cell in the ovary of MRL/MpJ 1* (*mcom1*) and *mcom2*, respectively.

Suggestive QTL for SEMC ratio were mapped to C57BL/6N-type *D4Mit42* (LRS = 6.6, 82.64 cM) and MRL/MpJ-type *D9Mit18* (LRS = 6.4, 71.49 cM) (Fig. 2-4E, Table 2-3), while a significant QTL was mapped to MRL/MpJ-type *D8Mit89* (LRS = 12.6, 62.93 cM), which overlapped with *mcom2* (Fig 2-4F, J, Table 2-3).

Analysis of epistatic interactions involved in OMC appearance

Epistatic interactions were examined to determine QTL responsible for the appearance of OMCs. QTL interaction was identified between *D8Mit312* (47.12 cM) and *D6Mit74* (23.70 cM) for both OMC and SEMC densities. Additional QTL interactions were identified between *D8Mit248* (44.99 cM) and *D19Mit33* (51.76 cM) for SEMC density, and between *D8Mit89* (62.93 cM) and *D19Mit91* (40.53 cM) for SEMC ratio.

MRL/MpJ mice homozygous QTL on Chr 8 and heterozygous QTL on Chr 6 showed the highest values for OMC and SEMC densities, while QTL on Chr 6 had no effect on OMC number in mice with heterozygous QTL on Chr 8 (Fig. 2-5A, B). BMM mice carrying MRL/MpJ-type QTLs on Chrs 8 and 19 showed the highest values for SEMC density and SEMC ratio (Fig. 2-5C, D).

Evaluation of SNPs and expression level of candidate genes

Genes on the *mcom1* locus associated with MC migration and chemotaxis were

evaluated as candidates for the regulation of OMC density, because MCs were the only immune cell type present in the ovary of neonatal MRL/MpJ mice (Papadopoulos et al. 2000; Lee et al. 2003; Jackson et al. 2005; Juremalm et al. 2005; Tsunemi et al. 2006). SNPs of these genes were investigated in order to identify non-synonymous coding polymorphisms between MRL/MpJ and C57BL/6N mice using the SNP database available from the MPD. However, no non-synonymous coding polymorphisms were identified in MC migration- or chemotaxis-associated genes at *mcom1*, including Interleukin 15 (*Il15*), Matrix metallopeptidase 2 (*Mmp2*), Metallothionein 1–4 (*Mt1–Mt4*), Chemokine (C-C motif) ligand 17 (*Ccl17*), *Ccl22*, and Chemokine (C-X3-C motif) ligand 1 (*Cx3cl1*). In contrast, no genes associated with the MC migration or chemotaxis were reported at *mcom2*.

Expression levels of these MC chemoattractant genes at P0 were compared between MRL/MpJ and C57BL/6N ovaries by qPCR. *Mt4* and *Ccl17* expression were significantly higher in MRL/MpJ than in C57BL/6N mice, while *Il15* level was significantly lower in MRL/MpJ (Fig. 2-6A). Expression levels of other candidate genes were comparable between the two strains (Fig. 2-6A). Expression of *Ccl17*, but not *Mt4*, was positively correlated with that of the OMC marker gene, tryptase beta 2 (*Tpsb2*) in P0 MRL/MpJ mouse ovary (Fig. 2-6B, C).

Discussion

Influence of the maternal factors on OMC number

The appearance of OMCs varies according to mouse strain. In neonatal MRL/MpJ mice, OMCs are more abundant than in other strains, including C57BL/6N, and they are distributed beneath the ovarian SE. OMC density differed between MRLB6F1 and B6MRLF1, but was similar between F2 crosses, implying that maternally inherited mitochondrial haplotypes have no influence on this trait. These results led the author to hypothesize that maternal factors during pregnancy could affect the number of OMCs in perinatal mice. In contrast, no difference was found in SEMC ratio between direct and reciprocal F1 hybrids. In addition, SEMC ratio was not affected by the progesterone-induced delayed parturition in both MRL/MpJ and C57BL/6N mice, indicating that MC distribution beneath the ovarian SE was not regulated by parental strains.

In MRL/MpJ fetuses with artificially delayed parturition, OMC density at E21.5 was significantly higher than in age-matched mice at P2. Fetuses were exposed to high doses of steroid hormones during late pregnancy, and both of estradiol and progesterone levels have been shown to affect MC migration (Zierau et al. 2012). Although plasma levels of these hormones were measured as putative maternal factors affecting OMC number, no differences were detected between MRL/MpJ and C57BL/6N mice at E18.5 of normal pregnancy. Taken together, these findings indicate that maternal factors during pregnancy influences OMC number by altering the fetal environment through factors other than plasma steroid hormone levels.

Genetic regulation of OMC number

Because both the abundance of OMCs and their distribution beneath the ovarian SE were phenotypes unique to MRL/MpJ mice, three parameters were selected for QTL analysis: OMC and SEMC densities, as well as SEMC ratio. A high OMC density was correlated with the MRL/MpJ-type *D8Mit248–D8Mit312* on Chr 8 (*i.e.*, *mcom1* locus), whereas SEMC ratio was linked to a second locus, MRL/MpJ-type *D8Mit86–D8Mit89* on Chr 8 (*i.e.*, *mcom2*). These results clearly demonstrate that OMC abundance and distribution are regulated by independent genetic factors derived from *mcom1* and *mcom2*, respectively.

In addition, *D6Mit74* and *D19Mit91–D19Mit33* loci showed epistatic interactions with the *mcom1* and *mcom2*, respectively. The genotypes on these chromosomes affected the appearance of MCs only in mice carrying MRL/MpJ homozygosity at *mcom1* and *mcom2*. These results indicate that these loci on Chrs 6 and 19 are positive modifiers of *mcom1* and *mcom2*. QTL analysis using F2 progeny would be useful for identifying relevant loci on other chromosomes, and evaluating interactions between *mcom1* and *mcom2*.

Candidate genes affecting OMC number

The results of the QTL analysis suggested that genes at the *mcom1* locus could be major determinants of OMC number. Based on differences in gene expression between MRL/MpJ and C57BL/6N mice, two possible candidate genes were highlighted in *mcom1*: *Mt4* at 46.26 cM, and *Ccl17* at 46.85 cM on Chr 8. In contrast, no genes

associated with the MC migration or chemotaxis were located at *mcom2*, suggesting that other molecular mechanisms, such as non-coding RNA, could regulate MC distribution.

Ccl17 overexpression increases the number of MCs in chronic contact hypersensitivity, and *Ccl17*-deficient mice have reduced numbers of MCs in the skin (Tsunemi et al. 2006; Stutte et al. 2010). In the P0 ovary, *Ccl17* expression was upregulated in MRL/MpJ mice compared to C57BL/6N, and was positively correlated with the expression of the MC marker gene *Tpsb2*, suggesting *Ccl17* as a strong candidate gene at the *mcom1* locus.

Metallothioneins (MTs), comprising four subfamilies designated MT1 to MT4 in mammals, have ~85% homology to CCL17 at the amino acid level, and immune cells migrate chemotactically toward MT1 and MT2 (Yin et al. 2005). MT4 is expressed exclusively in stratified squamous epithelia such as oral epithelia, esophagus, and skin, where MCs are abundant (Quaife et al. 1994; Gersch et al. 2002). Interestingly, the expression of *Mt1* through *Mt4* was detected in the P0 ovary, but only *Mt4* was upregulated in MRL/MpJ mice relative to C57BL/6N, although no correlation was observed between the expression of *Mt4* and *Tpsb2*. Therefore, the overexpression of *Mt4* could induce MC migration in an all-or-none rather than a concentration-dependent manner.

Gene expression profiles in oocytes change dramatically during early follicular development, including immune response genes such as interleukins and chemokines (Kezele et al. 2005). The author reported a correlation between MC number and early follicular development in Chapter 1. Therefore, *mcom1* and *mcom2* would regulate the

early follicular development of neonatal mice by altering the appearance of OMC.

In summary, the appearance of OMCs was found to be closely associated with both environmental factors and filial genetic backgrounds. The environmental factors influenced the number but not the distribution of OMCs, but both were influenced by the filial genetic background and regulated by *mcom1* and *mcom2*, respectively. The identification of genes responsible for the appearance of OMCs helps to clarify the mechanisms underlying organ- and age-specific recruitment of MCs, and the role of these cells in early follicular development.

Summary

In MRL/MpJ mice, OMCs are more abundant than in other mouse strains, and tend to distribute beneath the ovarian SE at birth. The author investigated the factors regulating the appearance of neonatal OMCs in progeny of the crosses between MRL/MpJ and C57BL/6N strains. F1 neonates had less than half the number of OMCs than MRL/MpJ mice. Interestingly, MRLB6F1 had more neonatal OMCs than B6MRLF1, although they were distributed over comparable areas. Furthermore, in MRL/MpJ fetuses for which parturition was delayed until embryonic day 21.5, the number of OMCs was significantly higher than in age-matched controls at postnatal day 2. These results suggest that the number of OMCs was influenced by the environmental factors during pregnancy. QTL analysis using N2 backcross progeny revealed two significant loci on chromosome 8: *D8Mit343–D8Mit312* for the number of OMCs and *D8Mit86–D8Mit89* for their distribution, designated as *mast cell in the ovary of MRL/MpJ 1* (*mcom1*) and *mcom2*, respectively. Among MC migration-associated genes at *mcom1* locus, ovarian expression of chemokine (C-C motif) ligand 17 was significantly higher in MRL/MpJ than in C57BL/6N mice, and positively correlated with the expression of OMC marker genes. These results indicate that the appearance of neonatal OMCs in MRL/MpJ mice is controlled by environmental factors and filial genetic factors, and that the abundance and distribution of OMCs are regulated by independent filial genetic elements.

Tables and Figures

Table 2-1. Microsatellite markers used for genotyping.

Marker	cM	Marker	cM	Marker	cM	Marker	cM
D1Mit123	17.67	*D6Mit138*	1.81	*D9Mit90*	17.80	*D15Mit111*	13.02
D1Mit181	38.54	*D6Mit159*	12.36	*D9Mit302*	36.36	*D15Mit156*	32.19
D1Mit191	52.66	*D6Mit223*	21.81	*D9Mit76*	50.18	*D15Mit245*	48.21
D1Mit107	70.19	*D6Mit74*	23.70	*D9Mit18*	71.49		
D1Mit403	81.63	*D6Mit316*	27.41			*D16Mit131*	3.41
		D6Mit188	32.53	*D10Mit166*	2.06	*D16Mit59*	26.86
D2Mit369	24.51	*D6Mit10*	52.75	*D10Mit42*	39.72	*D16Mit140*	40.30
D2Mit249	54.07	*D6Mit194*	62.90	*D10Mit134*	54.72	*D16Mit106*	57.68
D2Mit340	73.59			*D10Mit271*	72.31		
D2Mit456	88.99	*D7Mit178*	2.02			*D17Mit113*	8.14
D2Mit148	100.49	*D7Mit82*	32.76	*D11Mit62*	5.78	*D17Mit139*	27.40
		D7Mit321	53.57	*D11Mit130*	27.28	*D17Mit119*	38.15
D3Mit182	21.73	*D7Mit105*	70.29	*D11Mit212*	54.34	*D17Mit221*	59.77
D3Mit244	35.01			*D11Mit48*	82.96		
D3Mit158	48.13	*D8Mit4*	18.89			*D18Mit177*	21.39
D3Mit350	63.88	*D8Mit226*	23.05	*D12Mit136*	13.00	*D18Mit51*	34.41
D3Mit129	80.49	*D8Mit8*	32.30	*D12Mit158*	38.14	*D18Mit186*	45.63
		D8Mit343	39.33	*D12Mit132*	57.68		
D4Mit235	3.57	*D8Mit50*	43.51			*D19Mit80*	18.24
D4Mit178	34.92	*D8Mit248*	44.99	*D13Mit17*	7.73	*D19Mit19*	34.08
D4Mit12	57.76	*D8Mit312*	47.12	*D13Mit13*	30.06	*D19Mit91*	40.53
D4Mit42	82.64	*D8Mit242*	50.07	*D13Mit191*	45.05	*D19Mit33*	51.76
		D8Mit313	55.07	*D13Mit260*	63.73		
D5Mit353	21.25	*D8Mit86*	56.18			*DXMit166*	28.26
D5Mit197	32.92	*D8Mit200*	61.37	*D14Mit11*	6.33	*DXMit25*	36.78
D5Mit240	53.24	*D8Mit89*	62.93	*D14Mit133*	16.80	*DXMit130*	55.45
D5Mit168	76.15	*D8Mit42*	74.46	*D14Mit141*	24.28	*DXMit186*	76.75
				D14Mit37	33.21		
				D14Mit266	64.86		

Table 2-2. Summary of the specific gene primers used in this chapter.

Gene	Forward Primer (5’-3’)	Reverse Primer (5’-3’)	Product size	Accession #
Il15	CATCCATCTCGTGCTACTTGTGTT	CATCTATCCAGTTGGCCTCTGTTT	126 bp	NM_008357
Mmp2	GGCTGGAACACTCTCAGGAC	CGATGCCATCAAAGACAATG	213 bp	NM_008610
Mt4	CTCAGCCTCCCTTTCTTAGC	ATCTCTCCCGCTGCCATAG	253 bp	NM_008631
Mt3	CCGGGAGGAACCAAGCTAC	GGGACACCCAGCACTATTTAC	293 bp	NM_013603
Mt2	TCTTCAAACCGATCTCTCGTC	GGCTAGGCTTCTACATGGTCT	289 bp	NM_008630
Mt1	GCTGTCCTCTAAGCGTCACC	GCTGGGTTGGTCCGATACT	324 bp	NM_013602
Ccl22	CCTGACGAGGACACATAACATC	TGGCAGAAGAATAGGGCTTG	380 bp	NM_009137
Cx3cl1	ATTGTCCTGGAGACGACACAG	TTGCCACCATTTTTAGTGAGG	119 bp	NM_009142
Ccl17	GAGTGCTGCCTGGATTACTTC	CGTCTCCAAATGCCTCAGC	215 bp	NM_011332
Tpsb2	CGACATTGATAATGACGAGCCTC	ACAGGCTGTTTTCCACAATGG	80 bp	NM_010781
Actb	TGTTACCAACTGGGACGACA	GGGGTGTTGAAGGTCTCAAA	165 bp	NM_007393

Table 2-3. Location of QTL for ovarian mast cells in BMM backcross progeny.

Chr.	Peak cM	Microsatellite Marker	OMC density			SEMC density			SEMC ratio		
			LRS	% variance	*P* value	LRS	% variance	*P* value	LRS	% variance	*P* value
2	73.59	*D2Mit340*				8.4	4	0.00333			
4	82.64	*D4Mit42*	7.0	4	0.00754				6.6	3	0.00958
8	44.99	*D8Mit248*	20.4**	10	0.00001						
	47.12	*D8Mit312*	20.4**	10	0.00001	24.5**	12	<0.00001			
	62.93	*D8Mit89*				15.9*	8	0.00007	12.6*	6	0.00039
9	71.49	*D9Mit18*							6.4	3	0.01238
13	7.73	*D13Mit17*				6.5	3	0.01138			
14	16.80	*D14Mit133*				8.1	4	0.00509			

LRS scores above the suggestive level are shown. *significant, **highly significant. OMC density: number of mast cells per total ovarian area.

SEMC density: number of mast cells facing ovarian surface epithelium per total ovarian area. SEMC ratio: ratio of SEMC to OMC densities.

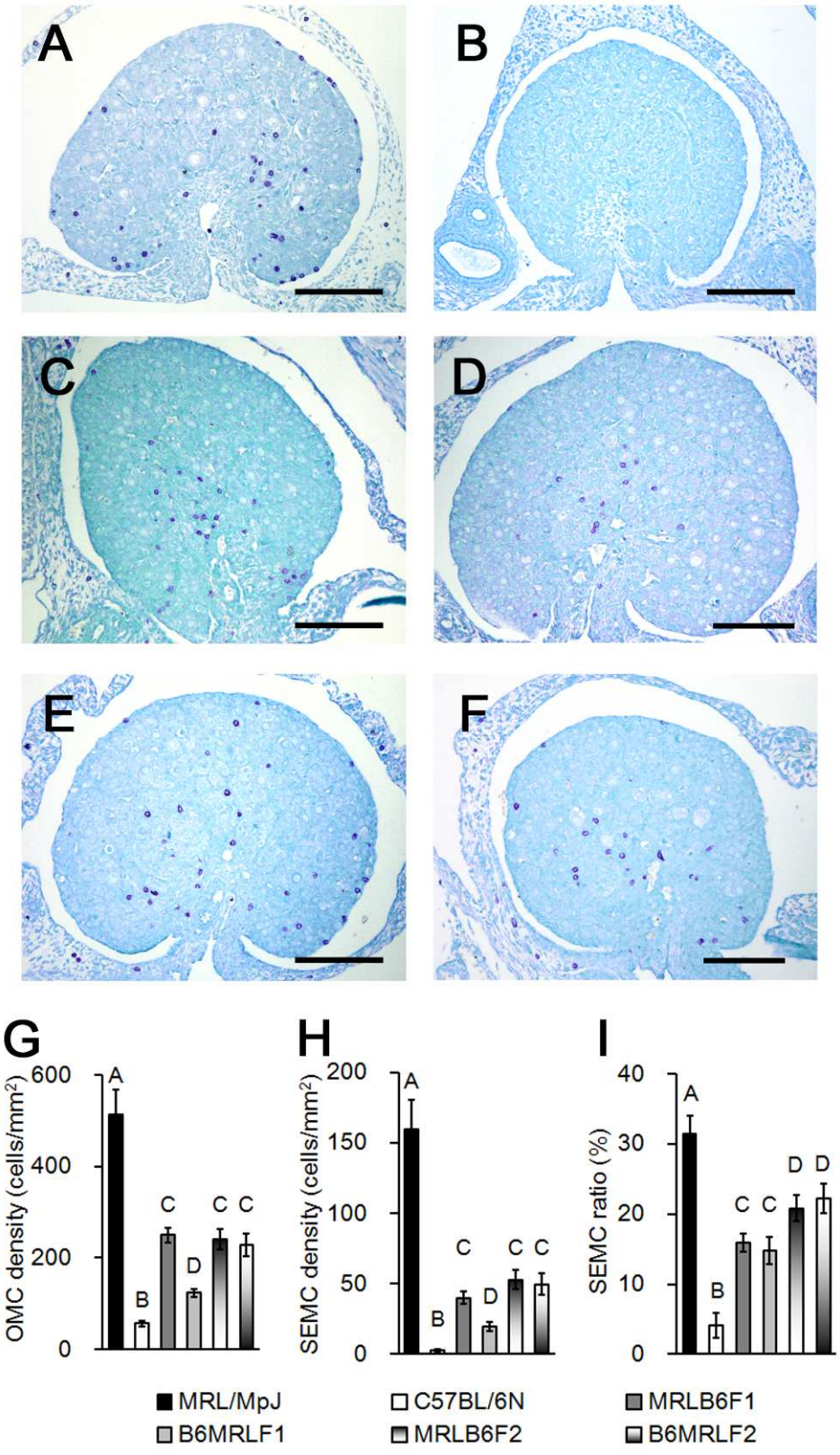
A
B
C
D
E
F
G
OMC density (cells/mm²)
600
400
200
0
A
B
C
D
C
C
H
SEMC density (cells/mm²)
200
150
100
50
0
A
B
C
D
C
C
I
SEMC ratio (%)
40
30
20
10
0
A
B
C
C
D
D
MRL/MpJ
B6MRLF1
C57BL/6N
MRLB6F2
MRLB6F1
B6MRLF2

Figure 2-1. Appearance of ovarian mast cells in MRL/MpJ and C57BL/6N mice, and F1 and F2 intercross mice at postnatal day 0.

(A–F) Toluidine blue-stained sections of ovaries in (A) MRL/MpJ, (B) C57BL/6N, (C) MRLB6F1, (D) reciprocal F1 (B6MRLF1), (E) MRLB6F2, and (F) reciprocal F2 (B6MRLF2). Bars: 100 μm. (G) Number of mast cells per total ovarian area (OMC density). (H) Number of mast cells facing ovarian surface epithelium per total ovarian area (SEMC density). (I) Ratio of SEMC density to OMC density (SEMC ratio). Data represent mean ± SEM (n = 10–20 per group). Significant differences were analyzed using Scheffé's method following the Kruskal-Wallis test. Statistical significance is indicated by different letters ($P < 0.05$).

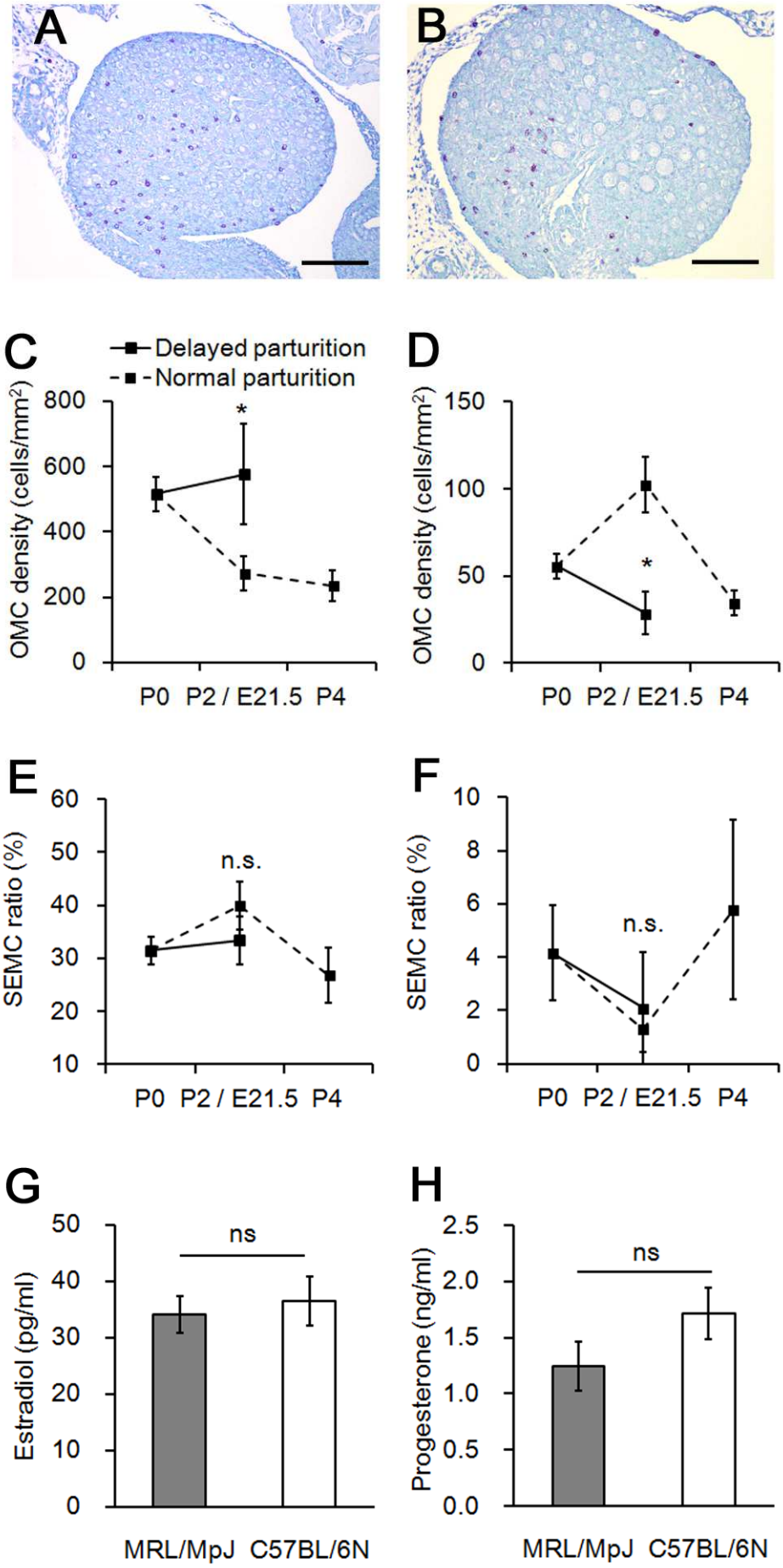
A
B
C
Delayed parturition
Normal parturition
OMC density (cells/mm2)
800
600
400
200
0
*
P0 P2 / E21.5 P4
D
OMC density (cells/mm2)
150
100
50
0
*
P0 P2 / E21.5 P4
E
SEMC ratio (%)
60
50
40
30
20
10
n.s.
P0 P2 / E21.5 P4
F
SEMC ratio (%)
10
8
6
4
2
0
n.s.
P0 P2 / E21.5 P4
G
Estradiol (pg/ml)
50
40
30
20
10
0
ns
MRL/MpJ C57BL/6N
H
Progesterone (ng/ml)
2.5
2.0
1.5
1.0
0.5
0.0
ns
MRL/MpJ C57BL/6N

Figure 2-2. Effect of delayed parturition on appearance of ovarian mast cells in MRL/MpJ and C57BL/6N mice.

(A and B) Toluidine blue-stained sections of MRL/MpJ mice ovaries at (A) embryonic day 21.5 with artificially delayed parturition, and (B) postnatal day 2. Bars: 100 μm. (C) Number of mast cells per total ovarian area (OMC density) in MRL/MpJ mice. (D) OMC density in C57BL/6N mice. (E) Ratio of number of mast cells facing ovarian surface epithelium per total ovarian area to OMC density (SEMC ratio) in MRL/MpJ mice. (F) SEMC ratio in C57BL/6N mice. (G) Plasma estradiol concentration at embryonic day 18.5. (H) Plasma progesterone concentration at embryonic day 18.5. Data represent mean ± SEM (n = 3–13 per group). Significant differences were analyzed using the Mann-Whitney *U* test. **P* < 0.05; ns, not significant.

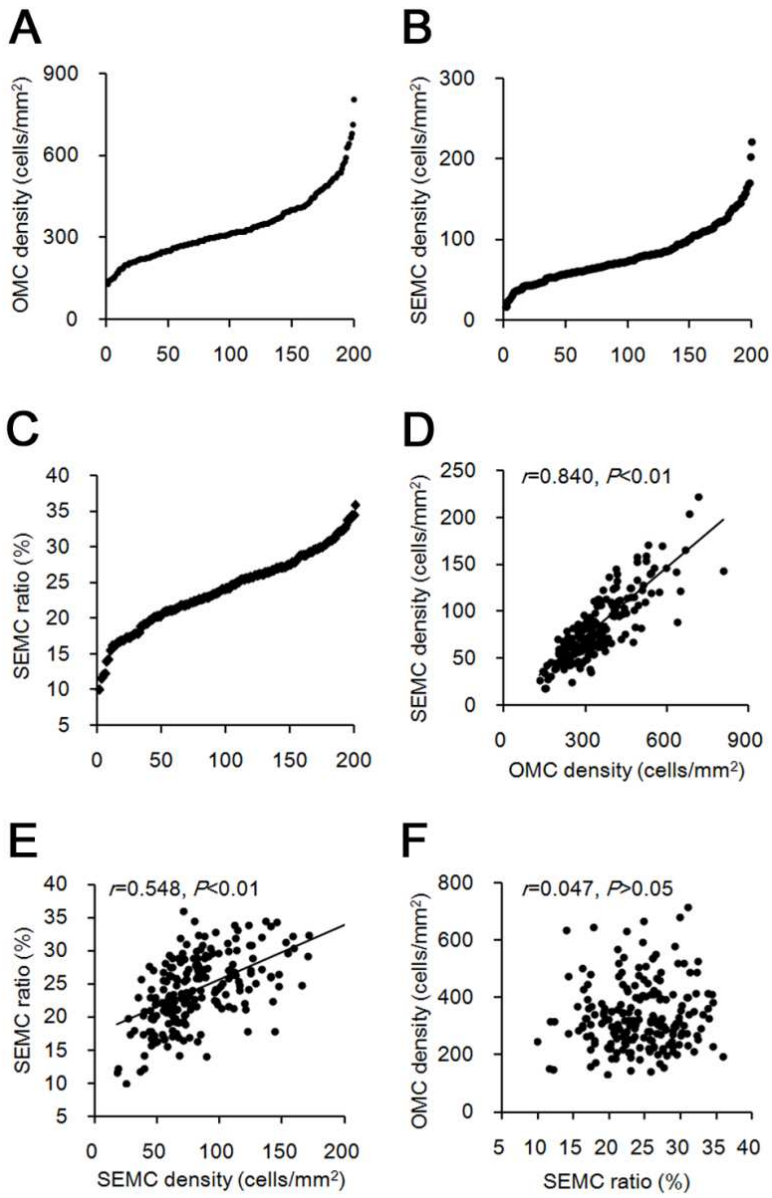

Figure 2-3. Appearance of ovarian mast cells in BMM progeny at postnatal day 0.

(A) Distribution of number of mast cells per total ovarian area (OMC density). (B) Distribution of number of mast cells facing ovarian surface epithelium per total ovarian area (SEMC density). (C) Distribution of ratio of SEMC to OMC densities (SEMC ratio). (D) Correlation between OMC and SEMC densities (Pearson's correlation test, n = 200). (E) Correlation between SEMC density and SEMC ratio (Pearson's correlation test, n = 200). (F) Correlation between SEMC ratio and OMC density (Pearson's correlation test, n = 200).

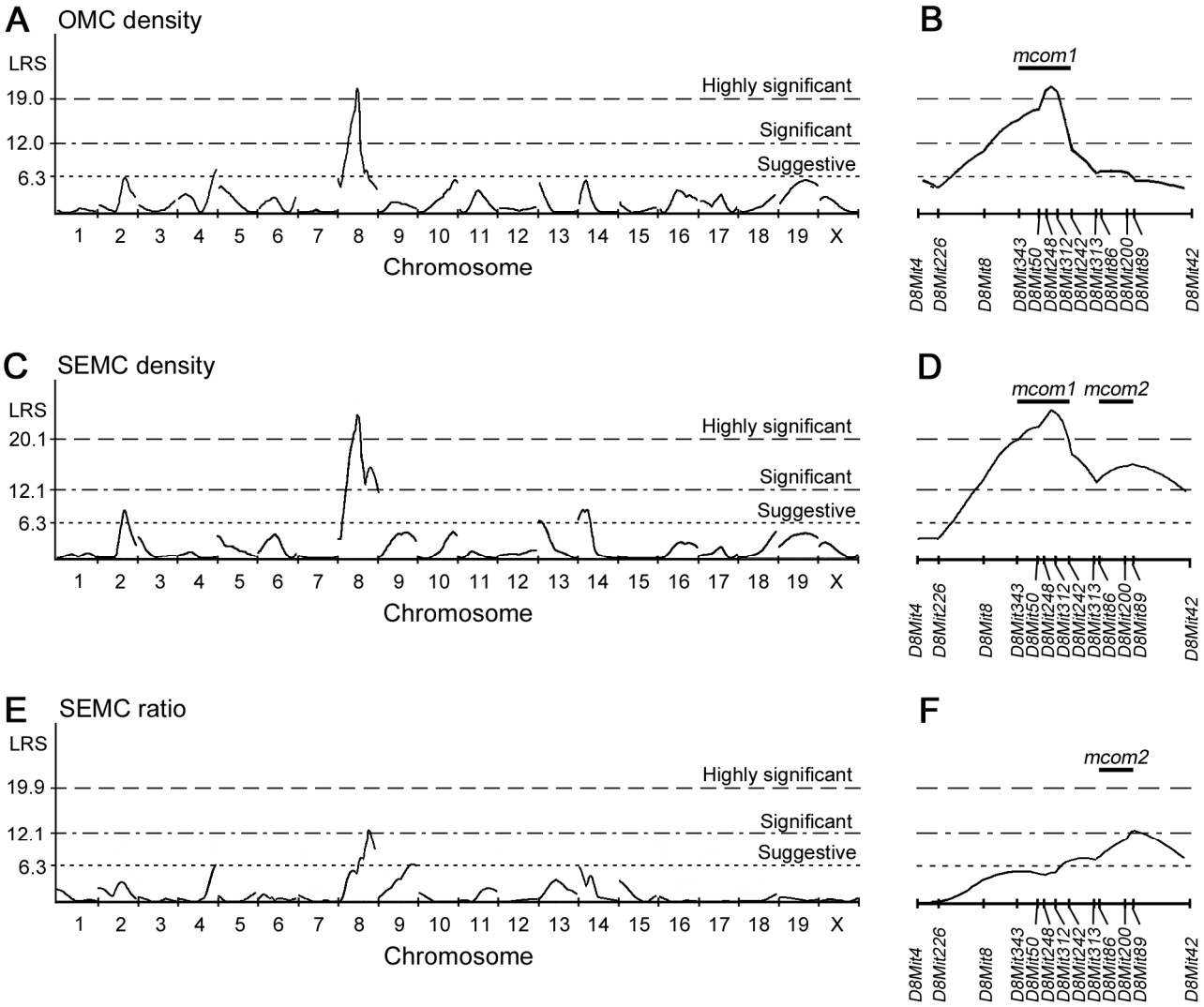
A
OMC density
LRS
19.0
12.0
6.3
Highly significant
Significant
Suggestive
1 2 3 4 5 6 7 8 9 10 11 12 13 14 15 16 17 18 19 X
Chromosome
B
mcom1
D8Mit4
D8Mit226
D8Mit8
D8Mit343
D8Mit50
D8Mit248
D8Mit312
D8Mit242
D8Mit313
D8Mit86
D8Mit200
D8Mit89
D8Mit42
C
SEMC density
LRS
20.1
12.1
6.3
Highly significant
Significant
Suggestive
1 2 3 4 5 6 7 8 9 10 11 12 13 14 15 16 17 18 19 X
Chromosome
D
mcom1 mcom2
D8Mit4
D8Mit226
D8Mit8
D8Mit343
D8Mit50
D8Mit248
D8Mit312
D8Mit242
D8Mit313
D8Mit86
D8Mit200
D8Mit89
D8Mit42
E
SEMC ratio
LRS
19.9
12.1
6.3
Highly significant
Significant
Suggestive
1 2 3 4 5 6 7 8 9 10 11 12 13 14 15 16 17 18 19 X
Chromosome
F
mcom2
D8Mit4
D8Mit226
D8Mit8
D8Mit343
D8Mit50
D8Mit248
D8Mit312
D8Mit242
D8Mit313
D8Mit86
D8Mit200
D8Mit89
D8Mit42
G
OMC density (cells/mm²)
500
400
300
200
A
B
M/B
M/M
D8Mit312
H
SEMC density (cells /mm²)
120
100
80
60
A
B
M/B
M/M
D8Mit312
I
SEMC density (cells /mm²)
120
100
80
60
A
B
M/B
M/M
D8Mit200
J
SEMC ratio (%)
30
28
26
24
22
20
A
B
M/B
M/M
D8Mit89

Figure 2-4. Quantitative trait loci linkage analysis for the appearance of ovarian mast cells.

(A) Interval mapping for number of mast cells per total ovarian area (OMC density). (B) Interval mapping on Chr 8 for OMC density. (C) Interval mapping for number of mast cells facing ovarian surface epithelium per total ovarian area (SEMC density). (D) Interval mapping on Chr 8 for SEMC density. (E) Interval mapping for ratio of OMC to SEMC densities (SEMC ratio). (F) Interval mapping on Chr 8 for SEMC ratio. (G) Allele effect of *D8Mit312* on OMC density. (H) Allele effect of *D8Mit312* on SEMC density. (I) Allele effect of *D8Mit200* on SEMC density. (J) Allele effect of *D8Mit89* on SEMC ratio. M/B indicates mice heterozygous with both a MRL/MpJ and C57BL/6N allele. M/M indicates mice homozygous for the MRL/MpJ allele. Data represent mean ± SEM. Significant differences were analyzed using the Mann-Whitney *U* test. Statistical significance is indicated by different letters ($P < 0.01$).

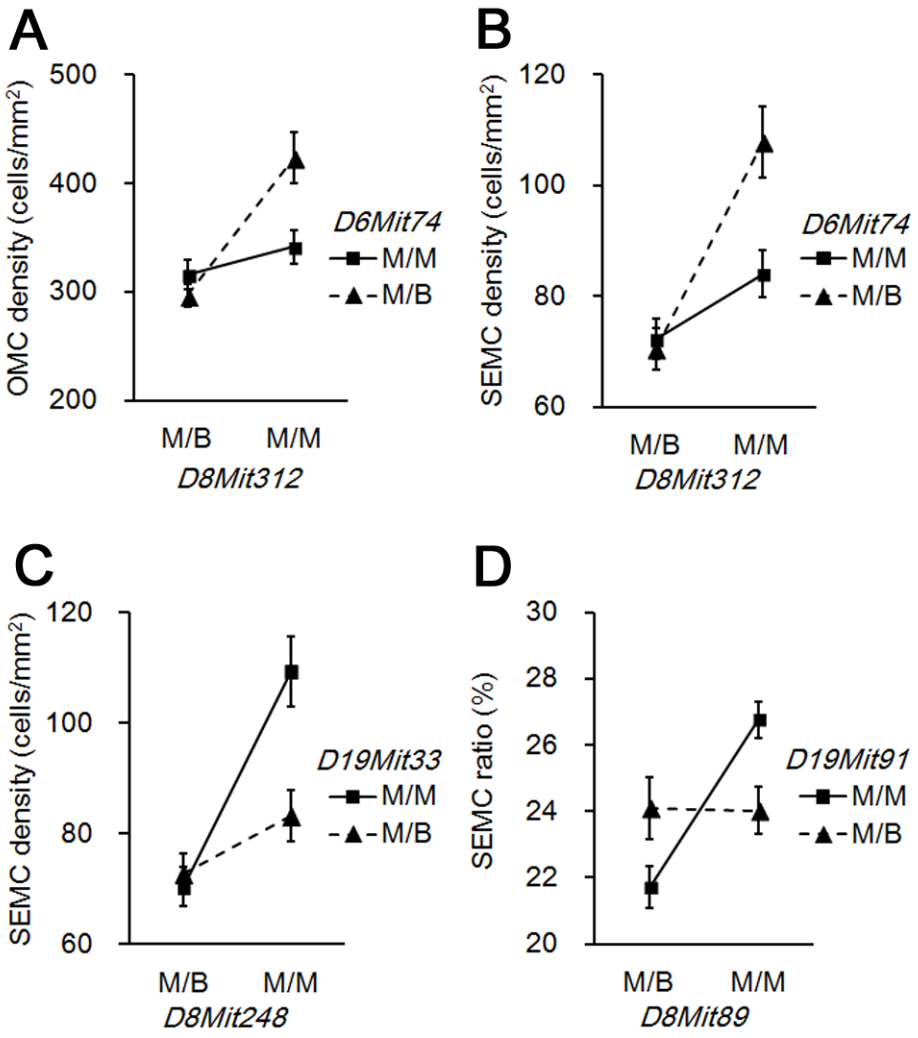

Figure 2-5. Epistatic interactions regulating the appearance of ovarian mast cells.

(A) Genotypic interactions between *D8Mit312* and *D6Mit74* for the number of mast cells per total ovarian area (OMC density). (B) Genotypic interactions between *D8Mit312* and *D6Mit74* for the number of mast cells facing ovarian surface epithelium per total ovarian area (SEMC density) (C) Genotypic interactions between *D8Mit248* and *D19Mit33* for SEMC density. (D) Genotypic interactions between *D8Mit89* and *D19Mit91* for SEMC ratio. M/B indicates mice heterozygous with both a MRL/MpJ and C57BL/6N allele. M/M indicates mice homozygous for the MRL/MpJ allele. Data represent mean ± SEM.

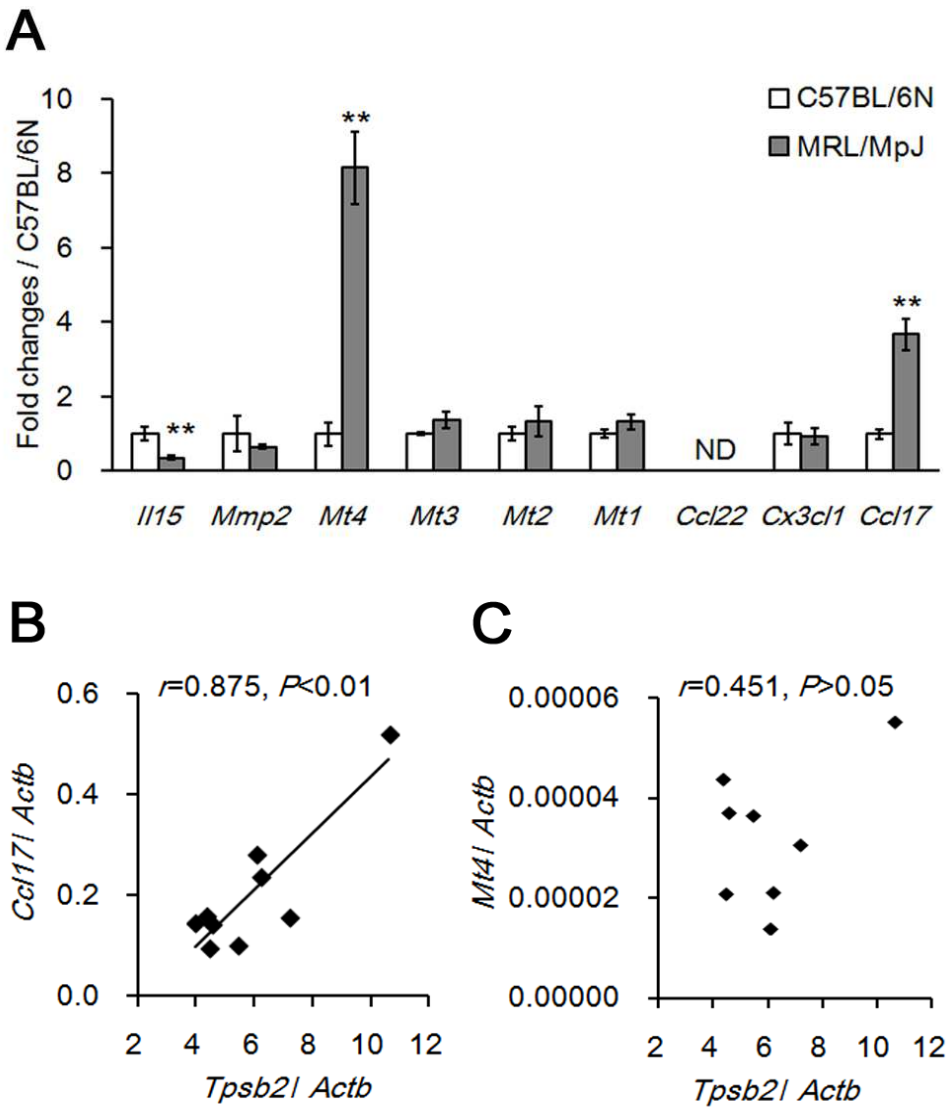

Figure 2-6. Candidate genes regulating the appearance of neonatal ovarian mast cells. (A) Quantitative real-time PCR analyses of candidate gene expression at postnatal day 0. Significant differences were analyzed using the Mann-Whitney *U* test. $^{**}P < 0.01$; ND, not detected. (B) Correlation between *Tpsb2* and *Ccl17* (Pearson's correlation test, n = 9). (C Correlation between *Tpsb2* and *Mt4* (Pearson's correlation test, n = 8).

Conclusion

Mast cells (MCs) reside in most tissues and act as sentinel cells in both innate and adaptive immunity. In several mammalian species including human, MCs are also present in the adult ovaries, and previous studies indicated that MCs play some roles in reproductive functions. Although a few MCs are found in the neonatal ovaries of ICR and C57BL/6N mice, the functional relationship between MCs and the perinatal ovary is unclear. In the thesis, the author found numerous ovarian MCs (OMCs) in neonatal MRL/MpJ mice, analyzed them with follicular development, and clarified the factors affecting their appearance.

In MRL/MpJ mice at postnatal day 0, the appearance of numerous MCs was an ovary-specific phenotype compared to C57BL/6N mice, and the MCs were the only immune cells abundantly present in the ovary. In MRL/MpJ mice, OMCs were most abundantly observed at postnatal day 0, and tended to localize adjacent to the SE. The appearance and localization of OMCs was dependent on the mouse strain. Specifically, the abundance of OMCs beneath the SE was a novel and unique phenotype of neonatal MRL/MpJ mice.

In MRL/MpJ mice, some OMCs migrated into the oocyte nests, and directly contacted the compressed and degenerated oocytes. MCs tended to localize beside the nest-stage oocyte rather than the primordial or primary follicle, and the number of oocytes in the nest was significantly lower than in the other mouse strains. Furthermore, the expression of follicle developmental markers was significantly higher in MRL/MpJ mice than in C57BL/6N mice, indicating that follicular development occurred earlier in

the former than in the latter strains. Thus, the appearance of numerous OMCs is a unique phenotype of neonatal MRL/MpJ mice, and OMCs would participate in the nest breakdown, and contribute to the acceleration of the early follicular development in MRL/MpJ mice.

The author next examined the factors regulating the appearance of neonatal OMCs using the crosses between MRL/MpJ and C57BL/6N mice. MRLB6F1 had more neonatal OMCs than B6MRLF1, although they were distributed over comparable areas. Furthermore, in MRL/MpJ mouse fetuses for which parturition was delayed, the number of OMCs was significantly higher than in age-matched controls of normal delivery. These results suggest that the number of OMCs was influenced by the environmental factors during pregnancy. Quantitative trait locus analysis using N2 backcross progeny revealed two significant loci on chromosome 8: *D8Mit343–D8Mit312* for the number of OMCs and *D8Mit86–D8Mit89* for their distribution, designated as *mast cell in the ovary of MRL/MpJ 1* (*mcom1*) and *mcom2*, respectively. Among MC migration-associated genes at *mcom1* locus, ovarian expression of chemokine (C-C motif) ligand 17 was significantly higher in MRL/MpJ than in C57BL/6N mice, and positively correlated with the expression of OMC marker genes. Thus, the appearance of neonatal OMCs in MRL/MpJ mice is controlled by environmental factors and filial genetic factors, and the abundance and distribution of OMCs are regulated by independent filial genetic elements.

In mice just after birth, the oocyte nests break apart into individual cells and become primordial follicles. During this process, called nest breakdown, only a subset

of oocytes survives and the remaining oocytes die. The author's results suggest that the numerous OMCs in MRL/MpJ mice participate in the nest breakdown, and contribute to progressed early follicular development, under the control of both the environmental factors and the genetic factors. Therefore, the author concluded that MC is a unique cell relating to the progression of early follicular development, and MRL/MpJ mice, which possess a novel phenotype "the appearance of numerous MCs in neonatal ovary", would be useful to clarify the close relationship between immune system and reproductive system through MCs.

References

1. Brännström, M., Mayrhofer, G. and Robertson, S.A. 1993. Localization of leukocyte subsets in the rat ovary during the periovulatory period. Biol. Reprod. 48: 277–286.
2. Cavender, J.L. and Murdoch, W.J. 1988. Morphological studies of the microcirculatory system of periovulatory ovine follicles. Biol. Reprod. 39: 989–997.
3. Clark, L.D., Clark, R.K. and Heber-Katz, E. 1998. A new murine model for mammalian wound repair and regeneration. Clin. Immunol. Immunopathol. 88: 35–45.
4. Coucouvanis, E.C., Sherwood, S.W., Carswell-Crumpton, C., Spack, E.G. and Jones, P.P. 1993. Evidence that the mechanism of prenatal germ cell death in the mouse is apoptosis. Exp. Cell Res. 209: 238–247.
5. Coussens, L.M., Raymond, W.W., Bergers, G., Laig-Webster, M., Behrendtsen, O., Werb, Z., Caughey, G.H. and Hanahan, D. 1999. Inflammatory mast cells up-regulate angiogenesis during squamous epithelial carcinogenesis. Genes Dev. 13: 1382–1397.
6. De Felici, M., Lobascio, A.M. and Klinger, F.G. 2008. Cell death in fetal oocytes: many players for multiple pathways. Autophagy 4: 240–242.
7. De Pol, A., Vaccina, F., Forabosco, A., Cavazzuti, E. and Marzona, L. 1997. Apoptosis of germ cells during human prenatal oogenesis. Hum. Reprod. 12: 2235–2241.
8. Epifano, O., Liang, L.F., Familari, M., Moos, M.C. Jr. and Dean, J. 1995. Coordinate expression of the three zona pellucida genes during mouse oogenesis.

Development 121: 1947–1956.

9. Galli, S.J., Kalesnikoff, J., Grimbaldeston, M.A., Piliponsky, A.M., Williams, C.M. and Tsai, M. 2005a. Mast cells as “tunable” effector and immunoregulatory cells: recent advances. Annu. Rev. Immunol. 23: 749–786.
10. Galli, S.J., Nakae, S. and Tsai, M. 2005b. Mast cells in the development of adaptive immune responses. Nat. Immunol. 6: 135–142.
11. Gaytán, F., Aceitero, J., Bellido, C., Sánchez-Criado, J.E. and Aguilar, E. 1991. Estrous cycle-related changes in mast cell numbers in several ovarian compartments in the rat. Biol. Reprod. 45: 27–33.
12. Gersch, C., Dewald, O., Zoerlein, M., Michael, L.H., Entman, M.L. and Frangogiannis, N.G. 2002. Mast cells and macrophages in normal C57/BL/6 mice. Histochem. Cell Biol. 118: 41–49.
13. Greenfeld, C., Roby, K., Pepling, M., Babus, J., Terranova, P. and Flaws, J.A. 2007. Tumor necrosis factor (TNF) receptor type 2 is an important mediator of TNF alpha function in the mouse ovary. Biol. Reprod. 76: 224–231.
14. Gurish, M.F., Friend, D.S., Webster, M., Ghildyal, N., Nicodemus, C.F. and Stevens, R.L. 1997. Mouse mast cells that possess segmented/multi-lobular nuclei. Blood 90: 382–390.
15. Heikkila, H., Latti, S., Leskinen, M., Hakala, J., Kovanen, P. and Lindstedt, K.A. 2008. Activated mast cells induce endothelial cell apoptosis by a combined action of chymase and tumor necrosis factor-α. Arterioscler. Thromb. Vasc. Biol. 28: 309–314.

16. Hunt, J.E., Stevens, R.L., Austen, K.F., Zhang, J., Xia, Z. and Ghildyal, N. 1996. Natural disruption of the mouse mast cell protease 7 gene in the C57BL/6 mouse. J. Biol. Chem. 271: 2851–2855.

17. Jackson, N.E., Wang, H.W., Tedla, N., McNeil, H.P., Geczy, C.L., Collins, A., Grimm, M.C., Hampartzoumian, T. and Hunt, J.E. 2005. IL-15 induces mast cell migration via a pertussis toxin-sensitive receptor. Eur. J. Immunol. 35: 2376–2385.

18. Jia, G., Cheng, G., Gangahar, D.M. and Agrawal, D.K. 2006. Insulin-like growth factor-1 and TNF-alpha regulate autophagy through c-jun N-terminal kinase and Akt pathways in human atherosclerotic vascular smooth cells. Immunol. Cell Biol. 84: 448–454.

19. Juremalm, M., Olsson, N. and Nilsson, G. 2005. CCL17 and CCL22 attenuate CCL5-induced mast cell migration. Clin. Exp. Allergy 35: 708–712.

20. Kerr, J.B., Duckett, R., Myers, M., Britt, K.L., Mladenovska, T. and Findlay, J.K. 2006. Quantification of healthy follicles in the neonatal and adult mouse ovary: evidence for maintenance of primordial follicle supply. Reproduction 132: 95–109.

21. Kezele, P.R., Ague, J.M., Nilsson, E. and Skinner, M.K. 2005. Alterations in the ovarian transcriptome during primordial follicle assembly and development. Biol. Reprod. 72: 241–255.

22. Kokubu, K., Hondo, E., Sakaguchi, N., Sagara, E. and Kiso, Y. 2005. Differentiation and elimination of uterine natural killer cells in delayed implantation and parturition mice. J. Reprod. Dev. 51: 773–776.

23. Kon, Y., Horikoshi, H. and Endoh, D. 1999. Metaphase-specific cell death in

meiotic spermatocytes in mice. Cell Tissue Res. 296: 359–369.

24. Kon, Y. and Endoh, D. 2000. Morphological study of metaphase-specific apoptosis in MRL mouse testis. Anat. Histol. Embryol. 29: 313–319.

25. Kon, Y. and Endoh, D. 2001. Heat-shock resistance in experimental cryptorchid testis of mice. Mol. Reprod. Dev. 58: 216–222.

26. Kon, Y., Konno, A., Hashimoto, Y. and Endoh, D. 2007. Ovarian cysts in MRL/MpJ mice originate from rete ovarii. Anat. Histol. Embryol. 36: 172–178.

27. Krishna, A., Beesley, K. and Terranova, P.F. 1989. Histamine, mast cells and ovarian function. J. Endocrinol. 120: 363–371.

28. Lätti, S., Leskinen, M., Shiota, N., Wang, Y., Kovanen, P.T. and Lindstedt, K.A. 2003. Mast cell-mediated apoptosis of endothelial cells in vitro: a paracrine mechanism involving TNF-α-mediated down-regulation of bcl-2 expression. J. Cell Physiol. 195: 130–138.

29. Lee, S.H., Ichii, O., Otsuka, S., Hashimoto, Y. and Kon, Y. 2010. Quantitative trait locus analysis of ovarian cysts derived from rete ovarii in MRL/MpJ mice. Mamm. Genome 21: 162–171.

30. Lee, Y.M., Kim, S.S., Kim, H.A., Suh, Y.J., Lee, S.K., Nahm, D.H. and Park, H.S. 2003. Eosinophil inflammation of nasal polyp tissue: relationships with matrix metalloproteinases, tissue inhibitor of metalloproteinase-1, and transforming growth factor-beta1. J. Korean Med. Sci. 18: 97–102.

31. Leferovich, J.M., Bedelbaeva, K., Samulewicz, S., Zhang, X.M., Zwas, D., Lankford, E.B. and Heber-Katz, E. 2001. Heart regeneration in adult MRL mice.

Proc. Natl. Acad. Sci. USA 98: 9830–9835.

32. Liu, J., Divoux, A., Sun, J., Zhang, J., Clément, K., Glickman, J.N., Sukhova, G.K., Wolters, P.J., Du, J., Gorgun, C.Z., Doria, A., Libby, P., Blumberg, R.S., Kahn, B.B., Hotamisligil, G.S. and Shi, G.P. 2009. Genetic deficiency and pharmacological stabilization of mast cells reduce diet-induced obesity and diabetes in mice. Nat. Med. 15: 940–945.

33. Lobascio, A., Klinger, F., Scaldaferri, M., Farini, D. and De Felici, M. 2007. Analysis of programmed cell death in mouse fetal oocytes. Reproduction 134: 241–252.

34. Manly, K.F., Cudmore, R.H. Jr. and Meer, J.M. 2001. Map Manager QTX, cross-platform software for genetic mapping. Mamm. Genome 12: 930–932.

35. Marcinkiewicz, J., Balchak, S. and Morrison, L. 2002. The involvement of tumor necrosis factor-α (TNF) as an intraovarian regulator of oocyte apoptosis in the neonatal rat. Front. Biosci. 7: d1997–d2005.

36. Namiki, Y., Endoh, D. and Kon, Y. 2003. Genetic mutation associated with meiotic metaphase-specific apoptosis in MRL/MpJ mice. Mol. Reprod. Dev. 64: 179–188.

37. Namiki, Y., Kon, Y., Kazusa, K., Asano, A., Sasaki, N. and Agui, T. 2005. Quantitative trait loci analysis of heat stress resistance of spermatocytes in the MRL/MpJ mouse. Mamm. Genome 16: 96–102.

38. Norman, R.J. and Brännström, M. 1994. White cells and the ovary – incidental invaders or essential effectors? J. Endocrinol. 140: 333–336.

39. Nose, M., Terada, M., Nishihara, M., Kamogawa, J., Miyazaki, T., Qu, W., Mori, S.

and Nakatsuru, S. 2000. Genome analysis of collagen disease in MRL/lpr mice: polygenic inheritance resulting in the complex pathological manifestations. Int. J. Cardiol. 75: S53–S61.

40. Otsuka, S., Konno, A., Hashimoto, Y., Sasaki, N., Endoh, D. and Kon, Y. 2008a. Oocytes in newborn MRL mouse testes. Biol. Reprod. 79: 9–16.

41. Otsuka, S., Konno, A., Hashimoto, Y., Sasaki, N., Endoh, D. and Kon, Y. 2008b. Polymorphism in MRL and AKR mice Sry: a candidate gene for the appearance of testicular oocyte. Jpn. J. Vet. Res. 56: 129–138.

42. Otsuka, S., Ichii, O., Namiki, Y., Sasaki, N., Hashimoto, Y. and Kon, Y. 2012. Genomic analysis of the appearance of testicular oocytes in MRL/MpJ mice. Mamm. Genome 11–12: 741–748.

43. Papadopoulos, E.J., Fitzhugh, D.J., Tkaczyk, C., Gilfillan, A.M., Sassetti, C., Metcalfe, D.D. and Hwang, S.T. 2000. Mast cells migrate, but do not degranulate, in response to fractalkine, a membrane-bound chemokine expressed constitutively in diverse cells of the skin. Eur. J. Immunol. 30: 2355–2361.

44. Pepling, M.E. and Spradling, A.C. 2001. Mouse ovarian germ cell cysts undergo programmed breakdown to form primordial follicles. Dev. Biol. 234: 339–351.

45. Quaife, C.J., Findley, S.D., Erickson, J.C., Froelick, G.J., Kelly, E.J., Zambrowicz, B.P. and Palmiter, R.D. 1994. Induction of a new metallothionein isoform (MT-IV) occurs during differentiation of stratified squamous epithelia. Biochemistry 33: 7250–7259.

46. Ramirez, R.A., Lee, A., Schedin, P., Russell, J.S. and Masso-Welch, P.A. 2012.

Alterations in mast cell frequency and relationship to angiogenesis in the rat mammary gland during windows of physiologic tissue remodeling. Dev. Dyn. 241: 890–900.

47. Robbie-Ryan, M. and Brown, M. 2002. The role of mast cells in allergy and autoimmunity. Curr. Opin. Immunol. 14: 728–733.

48. Rodrigues, P., Limback, D., McGinnis, L.K., Plancha, C.E. and Albertini, D.F. 2009. Multiple mechanisms of germ cell loss in the perinatal mouse ovary. Reproduction 137: 709–720.

49. Rudolph, M.I., Rojas, I.G. and Penissi, A.B. 2004. Uterine mast cells: a new hypothesis to understand how we are born. Biocell 28: 1–11.

50. Secor, V.H., Secor, W.E., Gutekunst, C.A. and Brown, M.A. 2000. Mast cells are essential for early onset and severe disease in a murine model of multiple sclerosis. J. Exp. Med. 191: 813–822.

51. Silva, C.A., Yamakami, L.Y., Aikawa, N.E., Araujo, D.B., Carvalho, J.F. and Bonfá, E. 2014. Autoimmune primary ovarian insufficiency. Autoimmun. Rev. 13: 427-430.

52. Skalko, R.G., Ruby, J.R. and Dyer, R.F. 1968. Demonstration of mast cells in the postnatal mouse ovary. Anat. Rec. 161: 459–463.

53. Stevens, R.L., Friend, D.S., McNeil, H.P., Schiller, V., Ghildyal, N. and Austen, K.F. 1994. Strain-specific and tissue-specific expression of mouse mast cell secretory granule proteases. Proc. Natl. Acad. Sci. USA 91: 128–132.

54. Stutte, S., Quast, T., Gerbitzki, N., Savinko, T., Novak, N., Reifenberger, J., Homey, B., Kolanus, W., Alenius, H. and Förster, I. 2010. Requirement of CCL17 for CCR7-

and CXCR4-dependent migration of cutaneous dendritic cells. Proc. Natl. Acad. Sci. USA 107: 8736–8741.

55. Takayama, T., Mishima, T., Mori, M., Jin, H., Tsukamoto, H., Takahashi, K., Takizawa, T., Kinoshita, K., Suzuki, M., Sato, I., Matsubara, S., Araki, Y. and Takizawa, T. 2005. Sexually dimorphic expression of the novel germ cell antigen TEX101 during mouse gonad development. Biol. Reprod. 72: 1315–1323.
56. Theofilopoulos, A.N. and Dixon, F.J. 1985. Murine models of systemic lupus erythematosus. Adv. Immunol. 37: 269–390.
57. Tsunemi, Y., Saeki, H., Nakamura, K., Nagakubo, D., Nakayama, T., Yoshie, O., Kagami, S., Shimazu, K., Kadono, T., Sugaya, M., Komine, M., Matsushima, K. and Tamaki, K. 2006. CCL17 transgenic mice show an enhanced Th2-type response to both allergic and non-allergic stimuli. Eur. J. Immunol. 36: 2116–2127.
58. Ugajin, T., Kojima, T., Mukai, K., Obata, K., Kawano, Y., Minegishi, Y., Eishi, Y., Yokozeki, H. and Karasuyama, H. 2009. Basophils preferentially express mouse mast cell protease 11 among the mast cell tryptase family in contrast to mast cells. J. Leukoc. Biol. 86: 1417–1425.
59. Welle, M. 1997. Development, significance, and heterogeneity of mast cells with particular regard to the mast cell-specific proteases chymase and tryptase. J. Leukoc. Biol. 61: 233–245.
60. Woidacki, K., Popovic, M., Metz, M., Schumacher, A., Linzke, N., Teles, A., Poirier, F., Fest, S., Jensen, F., Rabinovich, G.A., Maurer, M. and Zenclussen, A.C. 2013. Mast cells rescue implantation defects caused by c-kit deficiency. Cell Death Dis. 4:

e46.

61. Wulff, B.C., Parent, A.E., Meleski, M.A., DiPietro, L.A., Schrementi, M.E. and Wilgus, T.A. 2012. Mast cells contribute to scar formation during fetal wound healing. J. Invest. Dermatol. 132: 458–465.

62. Xing, W., Austen, K.F., Gurish, M.F. and Jones, T.G. 2011. Protease phenotype of constitutive connective tissue and of induced mucosal mast cells in mice is regulated by the tissue. Proc. Natl. Acad. Sci. USA 108: 14210–14215.

63. Yin, X., Knecht, D. and Lynes, M. 2005. Metallothionein mediates leukocyte chemotaxis. BMC immunol. 15: 6–21.

64. Yu, H., Mohan, S., Masinde, G.L. and Baylink, D.J. 2005. Mapping the dominant wound healing and soft tissue regeneration QTL in MRL × CAST. Mamm. Genome 16: 918–924.

65. Zierau, O., Zenclussen, A.C. and Jensen, F. 2012. Role of female sex hormones, estradiol and progesterone, in mast cell behavior. Front. Immunol. 3: 169.

Acknowledgements

First and foremost, I would like to express my gratitude towards my supervisor Dr. Yasuhiro Kon for his support, advice, and guidance throughout the duration of this project. I would like to thank Dr. Kazuhiro Kimura, Dr. Nobuya Sasaki, Dr. Masashi Nagano, and Dr. Osamu Ichii for time taken to provide advice, critical comments and assistance in completing this thesis. I would also like to thank Dr. Saori Otsuka and all the members of the laboratory of anatomy, and Dr. Ken-ichi Nagasaki and all member of the section of biological safety research, Japan food research laboratories for their encouragement, support, advice, and great times. Finally, I deeply appreciated to the animals supporting this study.

Conclusion in Japanese

MRL/MpJ マウスの新生子期卵巣に出現する肥満細胞の解析

–初期卵胞形成に参加する特異な免疫細胞–

北海道大学大学院獣医学研究科

比較形態機能学講座　解剖学教室

中村　鉄平

肥満細胞(MC)はほぼ全ての臓器に存在し、自然免疫及び獲得免疫において外来抗原に対する監視細胞として機能する。ヒトを含む数種の哺乳類において、MC は成体の卵巣にも存在し、MC と生殖機能との関連性が示唆されている。一方、新生子期のマウス卵巣にも少数の MC が存在するが、その機能的意義は不明である。本研究において、著者は MRL/MpJ マウスの新生子期卵巣に多数の MC を発見した。

生後 0 日齢 MRL/MpJ マウスの全身諸臓器のうち、MC 数は特に卵巣において C57BL/6N よりも有意に多かったが、いずれの系統でもマクロファージ、B 細胞、T 細胞、好中球及び好酸球は少数だった。新生子期において、MRL/MpJ マウスの卵巣内 MC (OMC) は生後 0 日齢で最も多く出現し、加齢と共に減少したのに加え、卵巣表面上皮と隣接して局在する傾向にあった。OMC の量及び局在はマウス系統に依存し、特に卵巣表面上皮直下に局在する MC 数は新生子 MRL/MpJ マウスで顕著に多かった。

MRL/MpJ マウスの新生子期卵巣において、一部の OMC は nest 内に存在し、圧迫又は変性した卵細胞に直接接していた。また、MRL/MpJ マウスでは、原始卵胞及び一次卵胞内の卵細胞と比較して nest 内の卵細胞と接する OMC が多く、nest 内の卵細胞数は他の系統より有意に少なかった。新生子期卵巣において、MRL/MpJ マウスの卵胞形成関連遺伝子の発現量は C57BL/6N マウスのそれより有意に高く、前者の卵胞形成は後者より進んでいることが示唆された。以上の形態学的観察結果より、多量の MC の出現及びその分布は MRL/MpJ マウスの新生子期卵巣に特徴的な表現型であり、本マウスの OMC は nest breakdown を介して初期の卵胞形成を早めている可能性が考えられた。

次いで、著者は MRL/MpJ と C57BL/6N マウスとの間で交雑系を作出し、新生子 OMC の出現を制御する因子を調査した。MRLB6F1 は B6MRLF1 と比較してより多くの OMC を有したが、その分布領域に差はなかった。更に、分娩を 2 日遅延させた MRL/MpJ マウス胎子の OMC 数は、通常分娩後 2 日齢の同マウスのそれより有意に多かった。

N2 戻し交配群を用いた QTL 解析の結果、significant レベルを超える QTL が Chromosome 8 の 2 箇所(OMC 数に関与する *D8Mit343–D8Mit312*、OMC の分布に関与する *D8Mit86–D8Mit89*)に検出され、それぞれ *mast cell in the ovary of MRL/MpJ 1* (*mcom1*)及び *mcom2* と命名した。*mcom1* に座位する MC 遊走関連遺伝子のうち、MRL/MpJ マウスの新生子期卵巣における chemokine (C-C motif) ligand 17 発現量は C57BL/6N マウスのそれより有意に高く、MRL/MpJ マウスでは OMC マーカー遺伝子発現量と有意な相関が認められた。このように、MRL/MpJ マウスの新生子期卵巣における MC の出現は、妊娠中の環境因子及び

子由来の遺伝的因子により制御され、OMC の量及び分布は各々独立した遺伝的因子によって制御されていた。

新生子マウスにおいて、卵細胞を包含する nest は崩壊して個々の原始卵胞となる。このプロセスは nest breakdown と呼ばれ、一部の卵細胞のみが生存し残りの卵細胞は死滅する。本研究の結果より、MRL/MpJ マウスの新生子卵巣における多量の MC は環境因子及び遺伝的因子の制御下で nest breakdown に参加し、初期の卵胞形成を早めていることが示唆された。結論として、MC は初期の卵胞形成に関与する特異な免疫細胞であり、新生子期 MRL/MpJ マウスの表現型は MC を介した免疫機構と生殖機構の新たな機能的関連を示していると考察した。